# Interaction effects in a two-dimensional electron gas in a random magnetic field: Implications for composite fermions and the quantum critical point

T. A. Sedrakyan and M. E. Raikh
*Department of Physics, University of Utah, Salt Lake City, Utah 84112, USA*
(Received 14 December 2007; published 27 March 2008)

We consider a clean two-dimensional interacting electron gas subject to a random perpendicular magnetic field $h(\mathbf{r})$. The field is nonquantizing in the sense that $\mathcal{N}_h$, a typical flux into the area $\lambda_F^2$ in the units of the flux quantum ($\lambda_F$ is the de Broglie wavelength), is small, $\mathcal{N}_h \ll 1$. If the spatial scale $\xi$ of change of $h(\mathbf{r})$ is much larger than $\lambda_F$, the electrons move along semiclassical trajectories. We demonstrate that a weak-field-induced curving of the trajectories affects the interaction-induced electron lifetime in a singular fashion: it gives rise to the correction to the lifetime with a very sharp energy dependence. The correction persists within the interval $\omega \sim \omega_0 = E_F \mathcal{N}_h^{2/3}$ much smaller than the Fermi energy $E_F$. It emerges in the third order in the interaction strength; the underlying physics is that a small phase volume $\sim(\omega/E_F)^{1/2}$ for scattering processes involving *two* electron-hole pairs is suppressed by curving. An even more surprising effect that we find is that *disorder-averaged* interaction correction to the density of states $\delta\nu(\omega)$ exhibits *oscillatory* behavior periodic in $(\omega/\omega_0)^{3/2}$. In our calculations of interaction corrections, a random field is incorporated via the phases of the Green functions in the coordinate space. We discuss the relevance of the new low-energy scale for realizations of a smooth random field in composite fermions and in disordered phase of spin-fermion model of ferromagnetic quantum criticality.

DOI: 10.1103/PhysRevB.77.115353 PACS number(s): 73.40.Gk, 71.10.Pm, 71.10.Ay, 71.70.Di

## I. INTRODUCTION

Electron-electron interactions are strongly modified when electrons move diffusively.[1] The resulting enhancement of the interactions leads in two dimensions to a divergent correction to the density of states[1,2] $\delta\nu(\omega)$. When electrons move ballistically and are scattered by point impurities, the anomaly persists, although it has a different underlying scenario.[3]

Within this scenario, individual impurities (unlike the diffusive case[1,2]) are responsible for the ballistic zero-bias anomaly by virtue of the following process. Static screening of each impurity by the Fermi sea creates a Friedel oscillation of the electron density with a period $\lambda_F/2$, where $\lambda_F$ is the de Broglie wavelength. Then, the amplitude of combined scattering from the impurity and the Friedel oscillation, which it created, exhibits anomalous behavior[3] when the scattering angle is either 0 or $\pi$. The energy $\omega$ of the scattered electron measured from the Fermi level $E_F$ defines the angular interval, $\sim(\omega/E_F)^{1/2}$, within which the scattering is enhanced. This enhancement translates into $\delta\nu(\omega) \propto \ln \omega$ correction to the density of states.

In a diagrammatic language, creation of the Friedel oscillation is described by a static polarization bubble. We note in passing that the *same* polarization bubble at finite frequency $\omega$ is responsible for the lifetime of electron of energy $\sim\omega$ with respect to creation of an electron-hole pair.

It is known[4] that in perfectly clean electron gas, finite-range interactions do not cause *any* anomaly in $\delta\nu(\omega)$. Then, a natural question to ask is whether or not the anomalous behavior of $\delta\nu(\omega)$ holds when a weak disorder is not point-like, as in Ref. 3, but is instead smooth. Finding an answer to this question is the main objective of the present paper. For concreteness, we choose a particular case of two-dimensional (2D) electron gas in a smooth random magnetic field, although our main results apply to the arbitrary smooth disorder.

Historically, the interest to the problem of 2D electron motion in a random static magnetic field first emerged in connection with a gauge field description of the correlated spin systems.[5–7] Later, this interest was stimulated by the notion that electron density variations near the half-filling of the lowest Landau level reduces to random magnetic field acting on composite fermions.[8,9] Another motivation was the possibility to artificially realize an inhomogeneous magnetic field acting on 2D electrons.[10–18] For *noninteracting* electrons, this motion has been studied theoretically in Refs. 19–32. In this paper, we trace how the perturbation of electron motion by a smooth random field affects the interaction corrections to the single-particle characteristics of the electron gas.

In Refs. 5–7, the averaging over static random field was carried out with the help of the path integral approach originally employed for diffusively moving electrons in a noisy environment[33] (see also Refs. 34 and 35). A crucial fact that ensures the effectiveness of this approach is that the field is assumed to be $\delta$ correlated. In fact, the correlation radius must be even smaller than $\lambda_F$. However, in realizations[8–18] mentioned above, the spatial scale of change of the random field in much bigger than $\lambda_F$. This leads to a completely different, semiclassical picture of the electron motion, when only the paths close to the classical trajectories are relevant. In this paper, we consider only this limit. The semiclassical character of motion suggests the way in which to perform the averaging over disorder realizations. Namely, the equation of motion can be first solved for *a given* realization, while averaging over realizations is carried out at the last step. This order is opposite to Refs. 5–7, where averaging was carried out in the general expression for the Green function after it was cast in the form of a path integral.

 

It might seem counterintuitive that any smooth disorder could generate a low-frequency scale for the interaction effects. Indeed, a smooth random field (including magnetic) does not produce Friedel oscillations, which are required for the anomaly[3] to develop. In a formal language, there are no static bubbles in the diagrams for the interaction correction to the self-energy. More precisely, in the smooth random field, they are exponentially suppressed. We will, however, demonstrate that the low-frequency scale emerges from *dynamic bubbles* after they are modified by a smooth disorder.

The new low-$\omega$ scale shows up in the virtual processes involving *more than one* electron-hole pair, i.e., two or more bubbles. This is because the momenta of states involved in these processes are strongly correlated, as was first pointed out in Ref. 36. Namely, these momenta are either almost parallel or almost antiparallel to each other. It is this correlation in momenta directions that is affected by the smooth random magnetic field. By suppressing the correlation, the random field gives rise to the low-$\omega$ feature in $\delta\nu(\omega)$. Clearly, both the height and the width of the feature depend on the magnitude of the random field. The above argument makes it clear why the low-$\omega$ scale does not emerge on the level of a single bubble modified by the random field. The reason is that the single bubble describes excitation of a single pair; there is no strong restriction on the momentum directions in this process.

Once the mechanism of nontrivial interplay of smooth disorder and interactions is identified, the following questions arise: What is the shape of the anomaly in $\delta\nu(\omega)$? How does it depend on the strength and the correlation radius of the random field? To address these questions, we develop a systematic approach to the calculation of interaction corrections in a smooth random field. The key element of our approach is incorporating the action along the *curved* semiclassical trajectories into the phases of the Green functions. Our calculation reveals a surprising fact, which could not be expected on the basis of the above qualitative consideration. It turns out that *disorder-averaged* correction $\langle\delta\nu(\omega)\rangle$ exhibits an *oscillatory* behavior. Oscillations emerge when two pairs participating in one of the possible processes giving rise to $\delta\nu$ are strongly correlated with each other. As an example, consider the process involving creation of the electron-hole pair, rescattering within the pair, and its subsequent annihilation. In this process, oscillations come from electron-electron scattering events that happen at the points located on a *straight line* and at equal distances. This is an example when disorder does not suppress but, on the contrary, *brings about* the oscillations.

Therefore, as we demonstrate in this paper, anomaly in the density of states is created by smooth spatial variation of the magnetic field, even though this variation does not produce Friedel oscillations. Although modification of the Friedel oscillations from a pointlike impurity by a smooth random field is not directly related to our situation with no impurities, this problem is still useful for gaining a qualitative understanding. Indeed, the relevant random-field-induced length scales, in our clean case, emerge in this problem as well. For this reason, we start with the study of suppression of the Friedel oscillations by the random field before the analysis of the interaction corrections in the random field.

We are not aware of literature on disorder-induced smearing of the Friedel oscillations.[37] However, a closely related issue of smearing of Ruderman-Kittel-Kasuya-Yoshida (RKKY) interaction between the localized spins by the disorder has a long history.[38–44] It is easy to see[38] that a short-range disorder suppresses exponentially the *average* RKKY interaction. However,[39–41] the average interaction does not represent the actual value of exchange in a *given realization*. This is due to the fast oscillations of the exchange with distance. The typical magnitude of the exchange can be inferred from the averaging of the *square* of the RKKY interaction;[39–41] this average is suppressed by the disorder only as a power law.

In this paper, we demonstrate that the decay of the *averaged* Friedel oscillations in the presence of a smooth disorder is quite nontrivial. In particular, when the field is strong enough, the average, in contrast to Ref. 38, falls off with distance as a power law. We would like to note that, recently, the notion of averaged Friedel oscillations became meaningful. This is because the possibility of visualization of a single-impurity-induced oscillation had been demonstrated experimentally.[45–53] The role of averaging can then be played by slow temporal fluctuations of the environment. Since experimental advances[45–53] were reported for correlated systems, recent theoretical studies[54–57] addressed the Friedel oscillations created by a *single* impurity in such systems.

The paper is organized as follows. In Sec. II, possible regimes of electron motion in a random magnetic field are identified. In Sec. III, we summarize our results on Friedel oscillations and interaction correction to the density of states for a *weak* random field, i.e., for the field in which the straight-line electron trajectories are weakly perturbed by the field. Subsequent Secs. IV–IX are devoted to the derivation of the results, outlined in Sec. III. Finally, in Sec. X, we translate our results into predictions for experimentally observable quantities in two prominent situations: composite fermions in half-field Landau level and electrons interacting with critical magnetic fluctuations near the quantum critical point. Details of some of the calculations are presented in Appendixes A–F.

## II. REGIMES OF ELECTRON MOTION IN A RANDOM MAGNETIC FIELD

Let $\mathbf{r}\equiv(x,y)$ be the coordinates of the 2D electron. The random magnetic field along the $z$ direction is characterized by the correlator

$$\langle h(\mathbf{r})h(\mathbf{r}')\rangle = h_0^2 K(|\mathbf{r}-\mathbf{r}'|/\xi), \quad K(0)\equiv 1, \qquad (2.1)$$

where $h_0$ is the rms magnetic field and $\xi$ is the correlation radius. Throughout this paper, we will assume that the random field is *slow fluctuating* in the sense that $\xi$ is much bigger than the de Broglie wavelength $\lambda_F$, the case opposite to the limit $\xi\to 0$ considered in Refs. 5–7. In terms of semiclassical description, different regimes of motion are classified according to the *classical* electron trajectory, which begins at the origin and ends at point $\mathbf{r}$. One should distinguish three different regimes, as illustrated in Fig. 1.

(i) Short-distance regime (regime I in Fig. 1). The trajec-

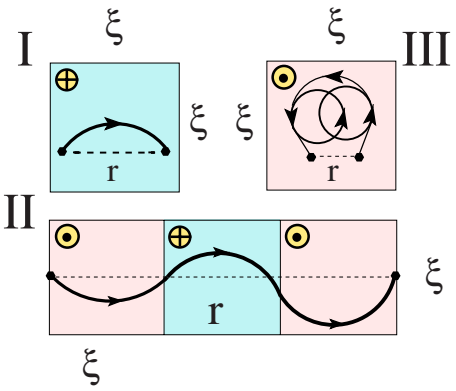


FIG. 1. (Color online) Types of semiclassical trajectories between two points separated by a distance $r$ in a random magnetic field: in regime I, the trajectories are of arc type; in regime II, the trajectories are of snake type; regime III corresponds to a drifting Larmour circle.

tory is of the *arc*-type. For this regime to be realized, two conditions must be met. Firstly, the change of magnetic field over the distance $r$ should be negligible, i.e., $r \ll \xi$. Secondly, the curving of electron trajectory in the *locally constant* magnetic field must be relatively small. The measure of this curving is $r/R_L$, where $R_L=\hbar c k_F/eh_0$ is the Larmour radius in the field $h_0$, and $k_F=2\pi/\lambda_F$ is the Fermi momentum. Thus, the short-distance regime corresponds to $r \ll \xi, R_L$.

(ii) "Weak-field" long-distance regime (regime II in Fig. 1). The trajectory is of the *snake* type. One condition for this regime is that the magnetic field changes sign many times within the distance $r$, i.e., $r \gg \xi$. The other is that within each interval of length $\sim\xi$, the curving of the trajectory is weak, i.e., $\xi \ll R_L$.

(iii) "strong-field" long-distance regime (regime III in Fig. 1). Electron executes many full Larmour circles before arriving to the point $\mathbf{r}$. The conditions for this regime are $R_L \ll r$ and $R_L \ll \xi$.

Note that the last two regimes correspond to the "semiclassical" and "strong" random magnetic field regimes in the language of Ref. 26. In order to accommodate all three regimes within a single diagram, it is convenient to introduce the dimensionless parameters

$$u = k_F R_L = (c\hbar k_F^2/eh_0) = \mathcal{N}_h^{-1},$$

$$v = r/R_L \sim k_F r \mathcal{N}_h, \tag{2.2}$$

where $\mathcal{N}_h < 1$ is the flux of the field $h_0$ into the area $\lambda_F^2$ (in the unites of the flux quantum). Then, regime I is defined by the lines $u=k_F\xi$ and $v=k_F\xi/u$, see Fig. 2. Regime III is separated from Regime I by the line $v=1$ and from regime II by the line $u=k_F\xi$. Finally, the dashed region $u<1$ in Fig. 2 corresponds to a quantizing magnetic field. The diagram in Fig. 2 is compiled for $k_F\xi \gg 1$, so it does not reflect the white-noise regime, $k_F\xi \ll 1$, of Refs. 5–7.

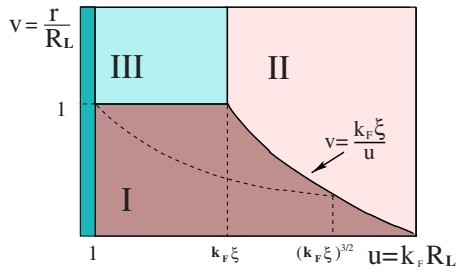


FIG. 2. (Color online) Parametric regions for regimes I, II, and III. The dashed line, $v=u^{-1/3}$, separates slow and fast *power-law* decays of the averaged Friedel oscillations within regime I: the oscillations fall off as $1/r^2$ to the left from the dashed line and as $1/r^{7/2}$ to the right from the dashed line.

## III. MAIN RESULTS

### A. Friedel oscillations

The simplest manifestation of the interplay of external field and electron-electron interactions shows up in spatial response of the electron gas to a pointlike impurity or, in other words, in Friedel oscillations. Denote with $U_{imp}(\mathbf{r})$ the short-range potential of the impurity. In the presence of interaction $V(\mathbf{r}-\mathbf{r}_1)$, the effective electrostatic potential in a clean electron gas falls off with $r$ as $V_H(r) \propto \sin(2k_F r)/r^2$ in a zero field. In Ref. 58, we had demonstrated that in a *constant* magnetic field $h=h_0$, this behavior modifies to

$$V_H(r) = -\frac{\nu_0 g V(2k_F)}{2\pi r^2} \sin\left[2k_F r - \frac{(p_0 r)^3}{12}\right], \tag{3.1}$$

where the characteristic momentum $p_0$ is defined as

$$p_0 = \frac{k_F}{(k_F R_L)^{2/3}} = \left(\frac{h_0}{k_F^{1/2}\Phi_0}\right)^{2/3}, \tag{3.2}$$

where $\Phi_0$ is the flux quantum. In Eq. (3.1) $\nu_0=m/\pi\hbar^2$ is the free electron density of states, $V(2k_F)$ is the Fourier component of $V(\mathbf{r})$, and the parameter $g$ is defined as $g=\int U_{imp}(\mathbf{r})d\mathbf{r}$. Equation (3.5) is valid within the domain $k_F^{-1} \lesssim r \lesssim R_L$, so that $(p_0 r)^3/12$ in the argument of sine does not exceed the main term $2k_F r$. As follows from Eq. (3.2), the characteristic length scale

$$r_1 = \frac{1}{p_0} = k_F^{1/3}\left(\frac{\Phi_0}{h_0}\right)^{2/3}, \tag{3.3}$$

defined by $p_0$ is intermediate between $R_L$ and $\lambda_F$, so that

$$R_L \gg r_1 \gg 1/k_F. \tag{3.4}$$

We see from Eq. (3.1) that only *the phase* of the Friedel oscillations is affected by the constant field, while the magnitude still falls off as $1/r^2$. The randomness of $h(x,y)$ results in randomness of the field-induced phase of the oscillations. This, in turn, translates into a faster decay of disorder-averaged oscillations. To quantify the behavior of the average $\langle V_H(r)\rangle$, we rewrite it in the form

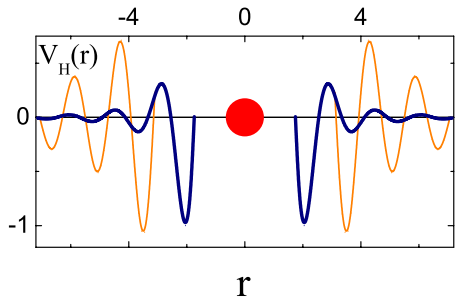


FIG. 3. (Color online) Friedel oscillations of the potential created by an impurity located at the origin. Thick line: averaged Friedel oscillations in regime I is plotted from Eqs. (3.5) and (3.6). Thin line: oscillations in the absence of the random field [Eq. (3.1) with $p_0=0$].

$$\langle V_H(r)\rangle = -\frac{\nu_0 g V(2k_F)}{2\pi r^2} F(r)\sin[2k_F r + \phi(r)], \qquad (3.5)$$

so that $F(r)$ describes the decay of the magnitude of the disorder-averaged oscillations. For a given distance $r$, the character of the phase randomization is different in regimes I and II. In regime I, we have $\xi \gg r$, and thus the relevant scale for the decay of $\langle V_H(r)\rangle$ is $r_\mathrm{I}$ (see Fig. 3). In Sec. V, we find that in this regime, the magnitude $F_\mathrm{I}$ and the phase $\phi_\mathrm{I}$ are the following functions of the dimensionless ratio $x=r/r_\mathrm{I}$:

$$F_\mathrm{I}(x) = \frac{1}{(1+x^6)^{1/4}},$$

$$\phi_\mathrm{I}(x) = -\arctan\left[\frac{\sqrt{1+x^6}-1}{x^3}\right]. \qquad (3.6)$$

In regime II, with snakelike trajectories (Fig. 1), the sign of the random field changes many, $\sim r/\xi \gg 1$, times within the distance $r$. As demonstrated in Sec. V, in this regime, we have

$$F_\mathrm{II}(x) = \frac{\sqrt{2}x}{\left[1+\frac{4}{9}x^4\right]^{1/2}\sqrt{\cosh^2 x - \cos^2 x}}, \qquad (3.7)$$

$$\phi_\mathrm{II}(x) = -\arctan\left[1-\frac{2}{1-\cot x \tanh x}\right] - \arctan\left[\frac{2}{3}x^2\right], \qquad (3.8)$$

where $x=r/r_\mathrm{II}$, with $r_\mathrm{II}$ defined as

$$r_\mathrm{II} = \eta\left(\frac{k_F}{\xi}\right)^{1/2}\frac{\Phi_0}{h_0}. \qquad (3.9)$$

In Eq. (3.9), the numerical factor $\eta$ depends on the functional form of the correlator Eq. (2.1) and will be defined in Sec. V.

In conclusion of this subsection, we point out that the actual character of the decay of Friedel oscillations with distance is governed by the following dimensionless combination of parameters, $h_0$ and $\xi$, in the correlator Eq. (2.1) of the random field:

$$\varepsilon = \frac{h_0^2\xi^3}{\Phi_0^2 k_F}. \qquad (3.10)$$

For $\varepsilon \gg 1$, i.e., for strong random field, the averaged oscillations decay with $r$ according to Eq. (3.6) in regime I. This is because for $\varepsilon \gg 1$, we have $p_0\xi \gg 1$. In the opposite limit of a weak random field $\varepsilon \ll 1$, we have $p_0\xi \ll 1$, so that the scale $p_0^{-1}$ is irrelevant, and, also, *no dephasing* takes place within the distance $\xi$. Thus, the characteristic decay length $r_\mathrm{II} \sim \xi/\varepsilon^{1/2}$ is much larger than $\xi$. This automatically guarantees that $k_F r_\mathrm{II} \gg 1$.

### B. Tunnel density of states

Two spatial scales, $r_\mathrm{I}$ and $r_\mathrm{II}$, define two energy scales,

$$\omega_0 = \frac{v_F}{r_\mathrm{I}} \sim E_F\left(\frac{h_0}{\Phi_0 k_F^2}\right)^{2/3} \sim E_F \mathcal{N}_h^{2/3},$$

$$\omega_1 = \frac{v_F}{r_\mathrm{II}} \sim E_F\left(\frac{\xi^{1/2}h_0}{k_F^{2/3}\Phi_0}\right) \sim E_F(k_F\xi)^{1/2}\mathcal{N}_h. \qquad (3.11)$$

As shown below, these scales manifest themselves in the anomalous behavior of the density of states in the *third order* in the electron-electron interaction parameter $\nu_0 V$. More specifically, in regime I, the bare density of states $\nu_0$ acquires a correction $\delta\nu_\mathrm{I}(\omega) \sim \nu_0(\nu_0 V)^3(\omega_0/E_F)^{3/2}\mathcal{I}(\omega/\omega_0)$, where $E_F$ is the Fermi energy. In regime II, the correction has a similar form $\delta\nu_\mathrm{II}(\omega) \sim \nu_0(\nu_0 V)^3(\omega_1/E_F)^{3/2}\mathcal{J}(\omega/\omega_1)$. Both functions $\mathcal{I}(z)$ and $\mathcal{J}(z)$ have characteristic magnitude and scale $\sim 1$. Moreover, they exhibit a quite "lively" behavior. In particular, a zero-bias anomaly $\delta\nu_\mathrm{I}(\omega)$ falls off at $\omega \gg \omega_0$ *with aperiodic oscillations*, i.e., $\mathcal{I}(z)$ has a contribution $\propto \sin(2^{8/3}\sqrt{3}z)z^{-3/4}\exp\{-2^{8/3}z\}$ for $z \gg 1$. The origin of the oscillations is the power-law decay of $F_\mathrm{I}(x)$, given by Eq. (3.6), and the brunch point, $x=e^{i\pi/6}$.

The contribution $\delta\nu_\mathrm{II}(\omega)$ also has a nonmonotonic behavior despite the fact that $F_\mathrm{II}(x)$ falls off exponentially as $\exp(-r/r\mathrm{II})$ [see Eq. (3.7)].

It is instructive to trace the evolution of the zero-bias anomaly upon increasing the magnitude of the random field $h_0$. This evolution is governed by parameter $\varepsilon$, Eq. (3.10). While $\varepsilon$ remains smaller than 1, where regime II applies, the anomaly is described by the function $\mathcal{J}(\omega/\omega_1)$ and broadens with $h_0$ as $v_F/r_\mathrm{II}(h_0) \propto h_0$. Upon further increasing $h_0$, when $\varepsilon$ exceeds 1, the crossover to regime I takes place. Zero-bias anomaly is then described by $\mathcal{I}(\omega/\omega_0)$; it broadens with $h_0$ as $v_F/r_\mathrm{I}(h_0) \propto h_0^{2/3}$ and *develops oscillations*. The fact that oscillations in $\delta\nu(\omega)$ *emerge* upon strengthening disorder might seem counterintuitive. This issue will be discussed in detail in Sec. VII.

In a zero magnetic field, an intimate relation between impurity-induced Friedel oscillations and the zero-bias anomaly was first established in Ref. 3. Namely, it was demonstrated that for short-range interaction, $\delta\nu(\omega)/\nu_0 \sim (\nu_0 V/E_F\tau)\ln\omega$, where $1/\tau = \nu_0\pi g^2 n_\mathrm{imp}$ is the electron scattering rate by the impurities, and $n_\mathrm{imp}$ is the impurity concentration. This anomaly is of the first order in $V$. A nontrivial question is whether or not the modification, Eq. (3.1), in a

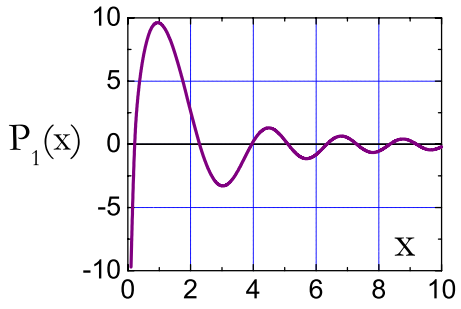


FIG. 4. (Color online) Magnetic-field-induced contribution Eq. (7.25) to the ballistic zero-bias anomaly Eq. (3.12). Field-dependent correction $[\delta\nu(\omega,h)-\delta\nu(\omega,0)]/\nu_0$ in the units $(\nu_0 V)^2(\omega_0/E_F)^{1/2}(E_F\tau)^{-1}$ is plotted versus dimensionless energy $2^{2/3}(\omega/\omega_0)$, where $\omega_0=(2E_F)^{1/3}\omega_c^{2/3}\gg\omega_c$, and $\omega_c$ is the cyclotron frequency.

*constant* magnetic field results in field dependence of the density of states in this order. In other words, whether or not a weak magnetic field introduces a cutoff of $\ln\omega$ at small $\omega$. The answer to this question is negative. In Ref. 58, it was demonstrated that the sensitivity of $\delta\nu(\omega)$ to a weak magnetic field indeed emerges but in the *second* order in $\nu_0 V$ (but still in the first order in $1/\tau$). The field-dependent correction $[\delta\nu(\omega,h)-\delta\nu(\omega,0)]/\nu_0$ has a characteristic frequency scale $\omega=\omega_0$. It is interesting to note that at $\omega\gg\omega_0$, this *impurity-induced* correction has an *oscillating* character:

$$\frac{\delta\nu(\omega,h)-\delta\nu(\omega,0)}{\nu_0}=\frac{(\nu_0 V)^2}{E_F\tau}\left(\frac{\omega_0}{E_F}\right)^{1/2}P\left(\frac{\omega}{\omega_0}\right). \quad (3.12)$$

The dimensionless function $P$ has the following large-$x$ asymptote:

$$P(x)\propto\frac{1}{x^{3/4}}\cos\left[\frac{8}{3\sqrt{3}}x^{3/2}-\frac{\pi}{4}\right]. \quad (3.13)$$

In Fig. 4, we show the oscillating correction to the density of states; the form of the function $P(\omega/\omega_0)$ is addressed in Sec. VII. Technically, the derivation of Eqs. (3.12) and (3.13) is quite analogous to the derivation of the oscillatory $\delta\nu$ in the random field in regime I. For this reason, we will outline this derivation in Sec. VII.

## IV. POLARIZATION OPERATOR IN A RANDOM MAGNETIC FIELD

Friedel oscillations $V_H(r)$ created by a pointlike impurity and the ballistic zero-bias anomaly originating from these oscillations[3] are intimately related to the Kohn anomaly in the polarization operator $\Pi(q)$ of a clean electron gas near $q=2k_F$. In two dimensions, this anomaly behaves as[59] $(q-2k_F)^{1/2}$, which translates into $1/r^2$ decay of the Friedel oscillations and $\propto\ln\omega$ correction to the density of states. Suppression of the Friedel oscillations $V_H(r)$ in a random field is a result of smearing of the Kohn anomaly in the momentum space. However, since the momentum is not a good quantum number in the presence of the random field, it is much more convenient to study the field-induced suppression of $V_H(r)$ directly in the coordinate space.

### A. Evaluation in the coordinate space

The polarization operator $\Pi_\Omega(\mathbf{r},\mathbf{r}')$ is defined in a standard way as

$$\Pi(\mathbf{r},\mathbf{r}',\Omega)=-i\int\frac{d\Omega'}{2\pi}G_{\Omega'}(\mathbf{r},\mathbf{r}')G_{\Omega-\Omega'}(\mathbf{r}',\mathbf{r}). \quad (4.1)$$

Here, $G_\Omega(\mathbf{r},\mathbf{r}')$ denotes causal Green function, which coincides with the retarded, $G^R_\Omega(\mathbf{r},\mathbf{r}')$, or advanced, $G^A_\Omega(\mathbf{r},\mathbf{r}')$, Green functions for $\Omega>0$ and $\Omega<0$, respectively. At distances $|\mathbf{r}-\mathbf{r}'|\gg k_F^{-1}$, the polarization operator in coordinate space represents the sums $\Pi_0(r,\omega)$ and $\Pi_{2k_F}(r,\omega)$ of slow and rapidly oscillating parts:

$$\Pi_0(r,\omega)=-\frac{i\pi\nu_0^2\hbar^4}{2k_F r}|\omega|\exp\left\{\frac{i|\omega|r}{v_F}\right\}, \quad (4.2)$$

$$\Pi_{2k_F}(r,\omega)=-\frac{\nu_0\hbar^3}{2r^2}\sin(2k_F r)A\left(\frac{2\pi rT}{v_F}\right)\exp\left\{\frac{i|\omega|r}{v_F}\right\}. \quad (4.3)$$

Subindices 0 and $2k_F$ emphasize that these parts come from small momenta and momenta close to $2k_F$ in $\Pi(q)$, respectively. Equation (4.2) emerges if one of the Green functions in Eq. (4.1) is retarded and the other is advanced. Equation (4.3) corresponds to the case when the Green functions in Eq. (4.1) are both advanced or both retarded.[60,61] Derivation of Eqs. (4.2) and (4.3) is presented in Appendix A. In Eq. (4.3), the function

$$A(x)=\frac{x}{\sinh x} \quad (4.4)$$

in $\Pi_{2k_F}$ describes the temperature damping.

### B. Qualitative derivation for the constant field

For a constant magnetic field $h(x,y)\equiv h_0$, the phase $\phi(r)$ in the argument of Eq. (3.5) can be inferred from the following simple qualitative consideration.

Classical trajectory of an electron in a weak magnetic field is curved due to the Larmour motion even at the spatial scales much smaller than $R_L$. As a result of this curving, the electron propagator $G(\mathbf{r}_1,\mathbf{r}_2)$ between the points $\mathbf{r}_1$ and $\mathbf{r}_2$ contains in the semiclassical limit a phase $k_F\mathcal{L}$, where $\mathcal{L}$ is the length of the arc of a circle with the radius $R_L$ that connects the points $\mathbf{r}_1$ and $\mathbf{r}_2$, see Fig. 5(a). Since the Friedel oscillations are related to the propagation from $\mathbf{r}_1$ to $\mathbf{r}_2$ *and back*, it is important that two arcs, corresponding to the opposite directions of propagation, define a *finite* area $\mathcal{A}$ so that the product $G(\mathbf{r}_1,\mathbf{r}_2)G(\mathbf{r}_2,\mathbf{r}_1)$ should be multiplied by the Aharonov–Bohm phase factor $\exp[ih_0\mathcal{A}/\Phi_0]$. Then, the phase of this product is equal to

$$2k_F r+\phi(r)=2k_F\mathcal{L}-\frac{h_0\mathcal{A}(\mathbf{r}_1,\mathbf{r}_2)}{\Phi_0}. \quad (4.5)$$

Simple geometrical relations, see Fig. 5(a), yield

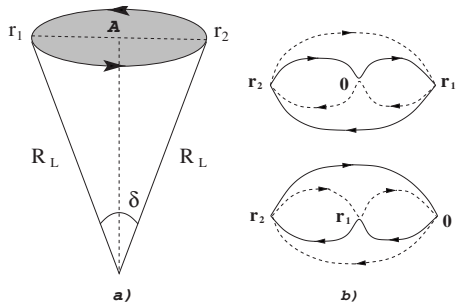


FIG. 5. (a) Origin of the net "magnetic" phase Eq. (4.7): two arcs, corresponding to the opposite directions of propagation, define a finite area $\mathcal{A}$. Aharonov–Bohm flux through this area makes the net phase *negative*. (b) Schematic illustration of the scattering processes giving rise to the additional phases Eqs. (7.6) and (7.7) in the product Eq. (7.5).

$$r = |\mathbf{r}_1 - \mathbf{r}_2| = 2R_L \sin(\delta/2),$$

$$\mathcal{L} = R_L\delta, \quad \mathcal{A} = 2R_L^2(\delta - \sin\delta). \tag{4.6}$$

Using this relation and assuming $r \ll R_L$, we find

$$\phi(r) = -\frac{h_0^2 r^3}{12k_F\Phi_0^2} = -\frac{(p_0 r)^3}{12}. \tag{4.7}$$

At this point, we would like to note that the conventional way[62] of incorporating a magnetic field into the semiclassical zero-field Green function amounts to multiplying it by $\exp[(1/\Phi_0)\int \mathbf{a}\cdot d\mathbf{l}]$, where the phase factor is the integral of the vector potential $\mathbf{a}$ along the straight line connecting the points $\mathbf{r}_1$ and $\mathbf{r}_2$. Such an incorporation neglects the field-induced curvature of the electron trajectories, and thus does not capture the modification Eq. (3.5) of the Friedel oscillations in the magnetic field. Indeed, the magnetic phase factors, introduced following Ref. 62, *cancel out* in the polarization operator.

With phase $\phi(r)$ given by Eq. (4.7), Friedel oscillations in a constant magnetic field acquire the form[58] of Eq. (3.1). To see this, we notice that with accuracy of a factor of $g/2\pi$ the potential, $V_H(r)$ coincides with $\Pi_{2k_F}(r,0)$. Then, the additional phase Eq. (4.7) transforms $\sin(2k_F r)$ into $\sin[2k_F r - (p_0 r)^3/12]$, as in Eq. (3.1).

In Appendix B, we present a rigorous derivation of Eq. (3.1) starting from *exact* electronic states in a constant magnetic field, as in Ref. 63.

### C. Field-induced phase of the Green function: Analytical derivation in a spatially inhomogeneous field

An additional semiclassical phase $\delta\varphi_{0\to\mathbf{r}}$ of the Green function due to the random magnetic field $h(x,y)$ is given by the following generalization of Eq. (4.7):

$$\delta\varphi_{0\to\mathbf{r}} = \frac{k_F}{2}\int_0^r dx\left(\frac{dy}{dx}\right)^2 - \frac{1}{\Phi_0}\int_0^r dx y(x)h(x,0), \tag{4.8}$$

where the first term comes from the elongation of the trajectory in the magnetic field. The second term describes the Aharonov–Bohm flux into the area restricted by the curve $y(x)$ and the $x$ axis. In Eq. (4.8), we assumed that the field does not change along the $y$ axis. This is the case when the maximal $y$ is smaller than the correlation radius $\xi$ of the random field. The condition $y < \xi$ is met in the regime of the arcs and the regime of the snakes, see Figs. 1 and 2.

In Eq. (4.8), we have also assumed that the magnitude of the de Broglie wavelength of the electron does not change along the trajectory. This can be justified from the equations of motion

$$m\frac{d^2y}{dt^2} = \frac{e}{c}h(x,0)\frac{dx}{dt},$$

$$m\frac{d^2x}{dt^2} = -\frac{e}{c}h(x,0)\frac{dy}{dt}. \tag{4.9}$$

It follows from Eq. (4.9) that the energy of electron $\frac{m}{2}[(dx/dt)^2 + (dy/dt)^2]$ is conserved even if the magnetic field changes with coordinates.

The most important step that allows to find $\delta\varphi_{0\to\mathbf{r}}$ analytically is that in regimes I and II in Fig. 1, we can replace $dx/dt$ by $v_F$ and set $t = x/v_F$ in the right-hand side of Eq. (4.9). This allows to replace $d^2y/dt^2$ by $v_F^2 d^2y/dx^2$. Then, the first of the equations yields

$$mv_F^2\frac{d^2y}{dx^2} = \frac{ev_F}{c}h(x,0). \tag{4.10}$$

By integrating this equation, we obtain

$$\frac{dy}{dx} = \frac{e}{mcv_F}\int_0^x dx' h(x',0) + C. \tag{4.11}$$

The constant $C$ should be found from the conditions $y(0) = 0$ and $y(r) = 0$, leading to

$$C = -\frac{e}{mcv_F r}\int_0^r dx'\int_0^{x'} dx'' h(x'',0) = -\frac{e}{mcv_F r}\int_0^r dx'\Lambda(x'), \tag{4.12}$$

where we have introduced an auxiliary function

$$\Lambda(x) = \int_0^x dx' h(x',0). \tag{4.13}$$

The meaning of $\Lambda(x)$ is the $y$ projection of the vector potential. By substituting Eq. (4.12) back into Eq. (4.11), we find

$$\frac{dy}{dx} = \frac{e}{mcv_F}\left[\int_0^x dx' h(x',0) - \frac{1}{r}\int_0^r dx'\int_0^{x'} dx'' h(x'',0)\right]$$
$$= \frac{e}{mcv_F}\left[\Lambda(x) - \frac{1}{r}\int_0^r dx\Lambda(x)\right]. \tag{4.14}$$

With the help of Eq. (4.14), one can express the first term in the additional phase Eq. (4.8) in terms of $\Lambda(x)$. It turns out that the second term in Eq. (4.8) exceeds twice the first term. To see this, one should multiply the first of the equations in Eq. (4.9) by $y(x)$ and integrate over $x$:

$$\int_0^r dx y(x)\frac{d^2y}{dx^2} = \frac{1}{\Phi_0 k_F}\int_0^r dx h(x,0)y(x). \tag{4.15}$$

The right-hand side of Eq. (4.15) is the second term in Eq. (4.8). The left-hand side of Eq. (4.15) can be related to the first term in Eq. (4.8) upon integration by parts:

$$\int_0^r dx y(x)\frac{d^2y}{dx^2} = -\int_0^r dx\left(\frac{dy}{dx}\right)^2. \tag{4.16}$$

Finally, we get

$$\delta\varphi_{0\to\mathbf{r}} = -\frac{k_F}{2}\int_0^r dx\left(\frac{dy}{dx}\right)^2 = -\frac{1}{\Phi_0^2 k_F}\left(\int_0^r dx\Lambda^2(x) - \frac{1}{r}\left[\int_0^r dx\Lambda(x)\right]^2\right). \tag{4.17}$$

It is convenient to rewrite the final result Eq. (4.17) directly in terms of the random field $h(\mathbf{r})$. By substituting Eq. (4.13) into Eq. (4.17), we obtain

$$\delta\varphi_{0\to\mathbf{r}} = \frac{1}{\Phi_0^2 k_F \xi}\int d\mathbf{r}_1 \int d\mathbf{r}_2 h(\mathbf{r}_1)\mathcal{R}(\mathbf{r}_1,\mathbf{r}_2)h(\mathbf{r}_2), \tag{4.18}$$

where the dimensionless kernel $\mathcal{R}(\mathbf{r}_1,\mathbf{r}_2)$ is defined as

$$\mathcal{R}(\mathbf{r}_1,\mathbf{r}_2) = \xi\delta(y_1)\delta(y_2)\left[r - \frac{x_1x_2}{r} - x_2\theta(x_2-x_1) - x_1\theta(x_1-x_2)\right]. \tag{4.19}$$

Note that for the constant field $h(x,y)=h_0$, evaluation of Eq. (4.18) using the kernel Eq. (4.19) reproduces the result Eq. (4.7), as expected.

## V. DISORDER-SMEARED FRIEDEL OSCILLATIONS IN DIFFERENT REGIMES

Smearing of the Friedel oscillations in the random field $h(\mathbf{r})$ originates from the randomness of the phase $\varphi_{0\to\mathbf{r}}$, which is related to $h(\mathbf{r})$ via Eqs. (4.18) and (4.19). Quantitatively, the magnitude $F(r)$ and the phase $\phi(r)$ of smeared Friedel oscillations Eq. (3.5) are determined by the following averages:

$$\Upsilon_1(r) = \mathrm{Im}\,\langle e^{2i\delta\varphi_{0\to\mathbf{r}}}\rangle_{h(\mathbf{r})}, \quad \Upsilon_2(r) = \mathrm{Re}\langle e^{2i\delta\varphi_{0\to\mathbf{r}}}\rangle_{h(\mathbf{r})}. \tag{5.1}$$

Then, $F(r)$ and $\phi(r)$ are related to the functions $\Upsilon_1(r)$ and $\Upsilon_2(r)$ as

$$F(r) = \sqrt{[\Upsilon_1(r)]^2 + [\Upsilon_2(r)]^2},$$

$$\phi(r) = \arctan\left[\frac{\Upsilon_1(r)}{\Upsilon_2(r)}\right]. \tag{5.2}$$

In this section, the averages in Eq. (5.1) will be calculated separately for the regime of arcs and the regime of snakes.

### A. Regime I

In the regime of arcs, we have $r \ll \xi$, so that the field is almost constant within the interval $(0,r)$ and is equal to its "local" value. For this reason, we can perform the averaging of $\exp[2i\varphi_{0\to\mathbf{r}}]$ over realizations of the random field $h(x,y)$ explicitly without specifying the form of the correlator $K(r/\xi)$. This is because we can first set $h(x,y)\equiv$const in $\exp[2i\varphi_{0\to\mathbf{r}}]$ and then make use of the fact that the distribution function of the local field is Gaussian.[64] The characteristic spatial scale $r_I$ for $F(r)$ and $\phi(r)$ immediately follows from Eq. (4.18) upon setting $h(0,r)=h_0$ and requiring $2\delta\varphi_{0\to\mathbf{r}}=1$. This yields $r_I = 2^{2/3}3^{1/3}/p_0$, where $p_0$ is given by Eq. (3.2).

#### 1. Random magnetic field

As discussed above, we start with Friedel oscillations in a constant *local* magnetic field $h$ for which we know that

$$F_I(r,h) = 1, \quad \phi_I(r,h) = -\epsilon_r\left(\frac{h}{h_0}\right)^2, \tag{5.3}$$

where $p_0 = k_F(\omega_c/E_F)^{2/3}$, and $\omega_c = eh_0/mc$ is the cyclotron frequency in the field $h_0$. In Eq. (5.3), the parameter $\epsilon_r$ is defined as

$$\epsilon_r = \frac{h_0^2 r^3}{12\Phi_0^2 k_F} = \frac{(p_0 r)^3}{12}. \tag{5.4}$$

To find the form of the averaged Friedel oscillation in regime I, in which $p_0\xi \ll 1$, we have to simply substitute the local value $h$ of the magnetic field into Eq. (3.1), i.e., replace $p_0^3$ by $p_0^3h^2/h_0^2$, and perform the Gaussian averaging over the distribution of the local field. This averaging can be carried out analytically with the use of the identity

$$\int_{-\infty}^{\infty}\frac{dx}{\sqrt{\pi}}e^{-x^2}\cos(\epsilon_r x^2+\beta) = \Upsilon_1(\epsilon_r)\cos\beta - \Upsilon_2(\epsilon_r)\sin\beta, \tag{5.5}$$

where the functions $\Upsilon_1$ and $\Upsilon_2$ for this case assume the following forms:

$$\Upsilon_1 \to \left(\frac{\pi}{2}\right)^{1/2}\sqrt{\frac{(1+\epsilon_r^2)^{1/2}+1}{1+\epsilon_r^2}}, \tag{5.6}$$

$$\Upsilon_2 \to \left(\frac{\pi}{2}\right)^{1/2}\sqrt{\frac{(1+\epsilon_r^2)^{1/2}-1}{1+\epsilon_r^2}}. \tag{5.7}$$

Using Eq. (5.2), we recover from Eqs. (5.6) and (5.7) the final result Eq. (3.6) for the magnitude $F_I(r/r_I)$ and the phase $\phi_I(r/r_I)$ of the Friedel oscillations in regime I.

In terms of variables $u$ and $v$ in the parametric space (Fig. 2), the condition $\epsilon_r=1$ can be presented as

$$v = \frac{1}{u^{1/3}}, \quad \text{where } u = k_F R_L, \quad v = \frac{r}{R_L}. \tag{5.8}$$

The dependence Eq. (5.8) is shown in Fig. 2 with a dashed line within regime I. To the left of this line, we have $\epsilon_r < 1$, so that $1/r^2$ decay of the Friedel oscillations is unchanged in

the random field. To the right of the dashed line, $\epsilon_r$ is bigger than 1. Then, the dependence $F(r) \propto \epsilon_r^{-1/2}$, which follows from Eq. (3.6), translates into faster *but still power-law* decay, $\propto 1/r^{7/2}$, of the Friedel oscillations. Note also that the phase of the oscillations also changes as $\epsilon_r$ crosses over from small to large values. Indeed, as follows from Eq. (3.6), we have $\phi(r) \to -\pi/4 + 1/(2r^3)$ in the limit $\epsilon_r \gg 1$.

#### 2. Periodic magnetic field

Consider a particular case of a *spatially periodic* magnetic field $h(x,y) = \tilde{h}_0 \cos(qx)$. For small enough $q$, the local description applies. The corresponding condition reads

$$q \ll \tilde{p}_0 = k_F \left( \frac{\tilde{h}_0}{k_F^2 \Phi_0} \right)^{2/3}. \tag{5.9}$$

Under this condition, the averaged Friedel oscillation can be found by averaging Eq. (3.1), in which $p_0$ is replaced by $\tilde{p}_0 (h/\tilde{h}_0)^{2/3}$, over the distribution $P(h)$ of the local values of the magnetic field rather than over the Gaussian distribution Eq. (5.5). This distribution has the form

$$P(h) = \frac{1}{\pi \sqrt{\tilde{h}_0^2 - h^2}}, \tag{5.10}$$

so that instead of Eq. (5.5), we have

$$\frac{1}{\pi} \int_{-1}^{1} dx \frac{\cos(\tilde{\epsilon}_r x^2 + \beta)}{\sqrt{1-x^2}} = J_0(\tilde{\epsilon}_r/2) \cos\left( \frac{\tilde{\epsilon}_r}{2} + \beta \right)$$

$$= \tilde{\Upsilon}_1(\tilde{\epsilon}_r) \cos\beta - \tilde{\Upsilon}_2(\tilde{\epsilon}_r) \sin\beta, \tag{5.11}$$

where $J_0$ is the Bessel function, $\tilde{\varepsilon}_r = (\tilde{p}_0 r)^3/12$, and

$$\tilde{\Upsilon}_1(\tilde{\epsilon}_r) = J_0\left( \frac{\tilde{\epsilon}_r}{2} \right) \cos\left( \frac{\tilde{\epsilon}_r}{2} \right),$$

$$\tilde{\Upsilon}_2(\tilde{\epsilon}_r) = J_0\left( \frac{\tilde{\epsilon}_r}{2} \right) \sin\left( \frac{\tilde{\epsilon}_r}{2} \right), \tag{5.12}$$

so that in a periodic field, instead of Eq. (3.6), we have

$$\tilde{F}(r) = [\tilde{\Upsilon}_1^2(\tilde{\epsilon}_r) + \tilde{\Upsilon}_2^2(\tilde{\epsilon}_r)]^{1/2} = \left| J_0\left( \frac{\tilde{\epsilon}_r}{2} \right) \right|,$$

$$\tilde{\phi}(r) = -\arctan\left[ \frac{\tilde{\Upsilon}_2(\tilde{\epsilon}_r)}{\tilde{\Upsilon}_1(\tilde{\epsilon}_r)} \right] = -\frac{\tilde{\epsilon}_r}{2}. \tag{5.13}$$

It is instructive to present the results Eq. (5.13) in a different form by simply showing how the Friedel oscillation Eq. (3.1) gets modified *on average* in the presence of a periodic magnetic field. By substituting Eq. (5.13) into Eq. (3.5), we get

$$\langle V_H(r) \rangle = -\frac{\nu_0 g V(2k_F)}{2\pi r^2} J_0\left( \frac{\tilde{p}_0^3 r^3}{24} \right) \sin\left[ 2k_F r - \frac{(\tilde{p}_0 r)^3}{24} \right]. \tag{5.14}$$

Equation (5.14) is a quite remarkable result. It suggests that, due to the periodic *smooth* magnetic field, the averaged Friedel oscillations *do not* get smeared. Rather, they acquire an *oscillatory envelope*, $J_0(\frac{\tilde{p}_0^3 r^3}{24})$. This envelope oscillates with "period"much larger than the de Broglie wavelength but *much smaller* than the period $1/q$ of change of the magnetic field.

Note that this effect provides a unique possibility to measure experimentally the *amplitude* of a periodic modulation. The reason is the following. The envelope Eq. (5.14) due to periodic magnetic field (or electric field, i.e., due to the lateral superlattice) translates into a distinct low-frequency behavior of the *tunnel density of states*. Namely, the tunnel density of states would exhibit an oscillatorybehavior with a period $\omega \sim \tilde{p}_0 v_F$. This period in $\omega$ depends only on the *magnitude* of the modulation $\tilde{h}_0$ but not on the spatial period of modulation, $2\pi/q$. Therefore, the magnitude of modulation, which, unlike the period, is hard to measure otherwise, can be inferred from the bias dependence of the tunneling conductance.

### B. Friedel oscillations in a random magnetic field: Regime II

As the magnitude $h_0$ of the random field decreases, the character of semiclassical motion changes from arclike (regime I in Fig. 1) to the snakelike (regime II in Fig. 1). To estimate for the "widths" $\delta y$ of the snakelike trajectories, we use Eq. (4.14) and set $x \sim \xi$. This yields

$$\frac{\delta y}{\xi} \sim \frac{e h_0 \xi}{m c v_F} \sim \left( \frac{\epsilon}{k_F \xi} \right)^{1/2}. \tag{5.15}$$

Since $k_F \xi \gg 1$ and $\epsilon \ll 1$ in regime II, we confirm that $\delta y \ll \xi$, i.e., that the snake is "narrow."

It is clear that at large enough distances $r$, the magnitude $F(r)$ of the averaged Friedel oscillations falls off exponentially with $r$. The prime question is what is the characteristic decay length. As stated in Sec. III, this length $r_{II}$ is given by Eq. (3.9). Below, we derive this length qualitatively and then establish the form of the magnitude $F_{II}(r)$ as well as the phase $\phi_{II}(r)$ for the average Friedel oscillations within the entire domain of $r$ by performing the functional averaging of $\exp(2i\delta\varphi_{0\to\mathbf{r}})$.

#### 1. Qualitative consideration

To recover qualitatively the scale $r_{II}$ from Eq. (4.18), we consider the following toy model. Let us divide the interval $(0,r)$ into small intervals of a *fixed* length $\xi$ (overall, $r/\xi$ intervals). Assume now that the random field takes only two values, $h_0$ and $-h_0$, each with probability 1/2 within a given interval $\xi$. Under this assumption, we find from Eq. (4.13) $\Lambda(r) = h_0[m(r) - n(r)]\xi$, where $m(r)$ and $n(r)$ are the numbers of small intervals within the length $r$, with $h = h_0$ and $h = -h_0$, respectively (obviously, $m+n = r/\xi$). From Eq. (4.17), we get for $\delta\varphi_{0\to\mathbf{r}}$

$$\delta\varphi_{0\to\mathbf{r}} = \frac{h_0^2\xi^2}{\Phi_0^2 k_F}\left\{\int_0^r dx[m(x)-n(x)]^2 - \frac{1}{r}\left(\int_0^r dx[m(x)-n(x)]\right)^2\right\}. \quad (5.16)$$

The second term in Eq. (5.16) is the square of the difference $\langle m\rangle - \langle n\rangle$ of coordinate (*not statistical*) average values of $m(x)$ and $n(x)$. Rewriting $m(x)$ as $\langle m\rangle + \delta m(x)$ and $n(x)$ as $\langle n\rangle + \delta n(x)$ and taking into account that $\delta m(x) + \delta n(x) = 0$, one can cast Eq. (5.16) into the form

$$\delta\varphi_{0\to\mathbf{r}} = \frac{4h_0^2\xi^2}{\Phi_0^2 k_F}\int_0^r dx[\delta m(x)]^2. \quad (5.17)$$

Since the typical value of $[\delta m(x)]^2$ is $\langle m(x)\rangle = x/2\xi$, we arrive at the estimate $\delta\varphi_{0\to\mathbf{r}} \sim h_0^2\xi r^2/\Phi_0^2 k_F$. Equating this additional phase to unity yields $r = \Phi_0 k_F^{1/2}/h_0\xi^{1/2}$, which coincides with $r_{\mathrm{II}}$ defined by Eq. (3.9) within a numerical factor.

### 2. Evaluation of the functional integral

Below, we present the analytical derivation of Eqs. (3.7) and (3.8). The averaging of $\exp(2i\delta\varphi_{0\to\mathbf{r}})$ required to calculate $F_{\mathrm{II}}(r)$ and $\phi_{\mathrm{II}}(r)$ from Eqs. (5.1) and (5.2) reduces to the functional integral

$$\langle e^{2i\delta\varphi_{0\to\mathbf{r}}}\rangle = \frac{\int D\{h(\mathbf{r})\}\exp[2i\delta\varphi(\mathbf{r}) - W\{h(\mathbf{r})\}]}{\int D\{h(\mathbf{r})\}\exp[-W\{h(\mathbf{r})\}]}, \quad (5.18)$$

where $\delta\varphi(r) = \delta\varphi_{0\to\mathbf{r}}$ is given by Eq. (4.17), and $\exp(-W\{h\})$ with $W\{h(\mathbf{r})\}$ given by

$$W\{h\} = \frac{1}{\xi^4 h_0^2}\int_0^{r_2}\int_{-\infty}^{\infty} dx_1 dy_1 \int_0^{r_2}\int_{-\infty}^{\infty} dx_2 dy_2 \times h(x_1,y_1)h(x_2,y_2)\kappa(x_1-x_2, y_1-y_2), \quad (5.19)$$

is the statistical weight of the realization $h(x,y)$. The dimensionless function $\kappa(\mathbf{r},\mathbf{r}')$ is related to the correlator Eq. (2.1) in a standard way:

$$\int d\mathbf{r}'\,\kappa(\mathbf{r},\mathbf{r}')K(\mathbf{r}',\mathbf{r}'') = \xi^4\delta(\mathbf{r}-\mathbf{r}''). \quad (5.20)$$

The reason why the functional integral Eq. (5.18) can be evaluated explicitly is that both $W\{h\}$ and $\delta\varphi_{0\to\mathbf{r}}$ are *quadratic* in the random field $h(x,y)$. The fact that we integrate over realizations of $h(x,y)$ defined on the interval which is *finite*, $0<x<r$, in the $x$ direction and infinite in the $y$ direction suggests the following expansion of $h(x,y)$:

$$h(x,y) = h_0\sum_{n=-\infty}^{\infty}\int_{-\infty}^{\infty} dq\mathcal{A}_{n,q}e^{iqy/\xi}\exp\left(\frac{2\pi i n x}{r}\right). \quad (5.21)$$

The asymmetry between $x$ and $y$ is quite significant in the calculation below, namely, for $r \gg \xi$, the characteristic values of $x$ turn out to be much larger than the characteristic values of $y$ if $\sim\delta y \ll \xi$, see Eq. (5.15). This allows to replace $K(x,y,x',y')$ in Eq. (5.20) by $\gamma\xi K(0,y-y')\delta(x-x')$, where the dimensionless constant $\gamma$ is defined by the relation

$$\gamma = \frac{\int_0^\infty dx\int_{-\infty}^\infty dy K(x,y)}{\xi\int_{-\infty}^\infty dy K(0,y)} = \left(\frac{\pi}{2}\right)\frac{\int_0^\infty dz z K(z)}{\int_0^\infty dz K(z)}, \quad (5.22)$$

where in the second identity, we used the fact that $K(x,y)$ is isotropic. Substituting Eq. (5.21) into Eq. (5.19), we obtain

$$W\{h\} = \frac{r}{\gamma\xi}\sum_{n=-\infty}^{\infty}\int dq\frac{|\mathcal{A}_{n,q}|^2}{\tilde{\mathcal{K}}(q)}, \quad (5.23)$$

where $\tilde{\mathcal{K}}(q)$ is the Fourier transform of the correlator, more precisely,

$$\tilde{\mathcal{K}}(q) = \frac{1}{\sqrt{2\pi}}\int\frac{dy}{\xi}e^{iqy/\xi}K(0,y). \quad (5.24)$$

The expression for $\delta\varphi(r)$ in terms of the coefficients $\mathcal{A}_{n,q}$ follows upon substitution of Eq. (B3) into Eq. (4.18):

$$\delta\varphi(r) = \frac{h_0^2}{\Phi_0^2 k_F}\sum_{n_1=-\infty}^{\infty}\sum_{n_2=-\infty}^{\infty}\int dq_1\mathcal{A}_{n_1,q_1}\int dq_2\mathcal{A}_{n_2,q_2}\int_0^r dx_1 \times\int_0^r dx_2\left[r - \frac{x_1x_2}{r} - x_2\Theta(x_2-x_1) - x_1\Theta(x_1-x_2)\right]\exp\left\{\frac{2\pi i}{r}(n_1x_1+n_2x_2)\right\}. \quad (5.25)$$

Performing the integration, we obtain

$$\delta\varphi(r) = \frac{\varepsilon r^3}{\xi^3}\left\{\frac{1}{12}\int dq\mathcal{A}_{0,q}^2 + \sum_{n>0}c_n\left|\int dq\mathcal{A}_{n,q}\right|^2 + \int dq\mathcal{A}_{0,q}\int dq\sum_{n>0}[b_n\mathcal{A}_{n,q} + b_n^*\mathcal{A}_{n,q}^*]\right\}, \quad (5.26)$$

where numerical coefficients $b_n$ and $c_n$ are defined as

$$b_n = -\frac{1}{2\pi^2n^2} + \frac{i}{2\pi n}, \quad c_n = \frac{1}{2\pi^2n^2}. \quad (5.27)$$

In writing the result of integration in the form of Eq. (5.26), we have used the dimensionless parameter $\varepsilon$ defined by Eq. (3.10). The meaning of this parameter is the additional phase Eq. (4.17), acquired by the electron traveling the distance $\sim\xi$ in a constant magnetic field $h_0$. Since our calculation pertains to the limit $r \gg \xi$, the relevant values of $\varepsilon$ are small.

The functional integration reduces now to the infinite product of the ratios of integrals over $\mathcal{A}_{n,q}$ and $\mathcal{A}_{n,q}^*$. The details of calculation are given in Appendix C. Here, we present only the final result for $r \gg \xi$:

$$\langle e^{2i\delta\varphi(r)}\rangle = \frac{1}{1-\frac{2i}{3}\left(\frac{r}{r_{\mathrm{II}}}\right)^2}\prod_{n=1}^{\infty}\frac{n^2}{n^2 - 2i(r/r_{\mathrm{II}})^2/\pi^2}, \quad (5.28)$$

where the characteristic length $r_{\mathrm{II}}$ is defined as

$$r_{\mathrm{II}} = \frac{2\xi}{[\sqrt{2\pi}\gamma\varepsilon]^{1/2}} = \sqrt{\frac{4k_F\Phi_0^2}{(2\pi)^{1/2}\gamma\xi h_0^2}}. \tag{5.29}$$

The above definition specifies the numerical coefficient $\eta$ in Eq. (3.9) of Sec. III as $\eta=2/(2\pi)^{1/4}\gamma^{1/2}$. This coefficient depends on the explicit form of the correlator via the factor $\gamma$, given by Eq. (5.22). It is seen that $r_{\mathrm{II}}\sim\xi/\varepsilon^{1/2}$ is indeed much larger than $\xi$. This means that, in regime II, Friedel oscillations survive well beyond the correlation radius of random magnetic field. Note also a distinctive dependence $r_{\mathrm{II}}\propto 1/h_0$ of the characteristic scale on the magnitude of the random field. In fact, the infinite product in Eq. (5.28) can be evaluated for arbitrary $r/r_{\mathrm{II}}$ using the identity

$$\frac{\sin x}{x} = \prod_n \left(1 - \frac{x^2}{\pi^2 n^2}\right), \tag{5.30}$$

which yields

$$\langle e^{2i\delta\varphi(r)}\rangle = \frac{1}{1-\frac{2i}{3}\left(\frac{r}{r_{\mathrm{II}}}\right)^2}\frac{(1+i)(r/r_{\mathrm{II}})}{\sin(r/r_{\mathrm{II}})\cosh(r/r_{\mathrm{II}}) + i\cos(r/r_{\mathrm{II}})\sinh(r/r_{\mathrm{II}})}. \tag{5.31}$$

With the help of Eq. (5.31), we can calculate the magnitude $F_{\mathrm{II}}(r)$ and the phase $\phi_{\mathrm{II}}(r)$ of the Friedel oscillations in regime II. Corresponding expressions are given by Eqs. (3.7) and (3.8).

#### 3. Limiting cases

It is not surprising that Friedel oscillations in regime II are smeared more efficiently than in regime I. The small-$r$ and the large-$r$ asymptotes of $F_{\mathrm{II}}(r)$ are the following:

$$F_{\mathrm{II}}(r) = 1 - \frac{11}{45}\left(\frac{r}{r_{\mathrm{II}}}\right)^4, \quad r \ll r_{\mathrm{II}}, \tag{5.32}$$

$$F_{\mathrm{II}}(r) = 3\sqrt{2}\left(\frac{r_{\mathrm{II}}}{r}\right)\exp\left(-\frac{r}{r_{\mathrm{II}}}\right), \quad r \gg r_{\mathrm{II}}. \tag{5.33}$$

We see from Eq. (5.33) that Friedel oscillations decay exponentially as $r$ exceeds $r_{\mathrm{II}}$. This should be contrasted to Eq. (3.6) for regime I, where the $F_{\mathrm{I}}(r)$ falls off slowly as $r^{-3/2}$ with $r$. On the qualitative level, the strong difference between regimes I and II, which is reflected in the different characters of decay of $F_{\mathrm{I}}(r)$ and $F_{\mathrm{II}}(r)$, is that in regime I, the random field does not change within the characteristic spatial interval $r_{\mathrm{I}}$, while in regime II, the sign of the random field changes many times within the characteristic spatial interval $r_{\mathrm{II}}$.

## VI. DENSITY OF STATES: QUALITATIVE DISCUSSION

In the previous consideration, we had demonstrated that in two regimes of electron motion in random magnetic field, i.e., regime of arcs, I, and regime of snakes, II, there are two length scales, $r_{\mathrm{I}}$ and $r_{\mathrm{II}}$, respectively, that govern the interaction effects. In this section, we demonstrate that the density of states $\delta\nu(\omega)$ exhibits an anomalous behavior within the frequency range $\omega\sim v_F/r_{\mathrm{I}}$ in the regime of arcs and $\omega\sim v_F/r_{\mathrm{II}}$ in the regime of snakes.

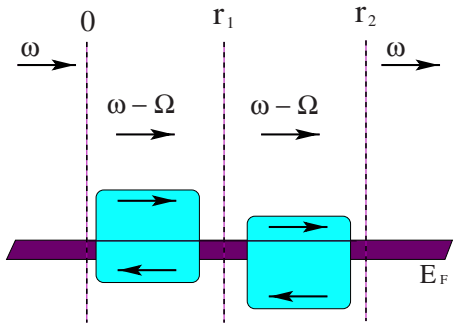


FIG. 6. (Color online) Third-order process describing creation of a pair by initial electron at point $\mathbf{r}=0$, rescattering within the pair at point $\mathbf{r}=\mathbf{r}_1$, and annihilation of the pair at point $\mathbf{r}=\mathbf{r}_2$. The diagram corresponding to this process is shown later in the text (the first diagram is in Fig. 8).

The process underlying the interaction corrections to the density of states is creation (and annihilation) of the virtual electron-hole pairs by an electron moving in the random field. Our central finding is that, unlike the case of pointlike impurities,[3] the low-$\omega$ structure in the density of states emerges as a result of electron-electron scattering processes involving *more than one pair*.

We start with a three-scattering process in the regime of arcs and demonstrate qualitatively how the frequency scale, $v_F/r_{\mathrm{I}}$, emerges. Three-scattering process involves *two* virtual pairs. Consider first this process in the absence of the random field. It is illustrated in Fig. 6. In the analysis of this process,[36,65,66] it was established that the directions of momenta of the participating electrons are strongly correlated, namely, they are either almost parallel or almost antiparallel. A quantitative estimate for the degree of alignment of the momenta can be obtained from inspection of Fig. 6. If the scattering acts take place at points 0, $\mathbf{r}_1$, and $\mathbf{r}_2$, then the corresponding matrix element contains a phase factor

$$\exp[2ik_F(r_1 - r_2 + |\mathbf{r}_1 - \mathbf{r}_2|)]. \tag{6.1}$$

This phase factor does not oscillate if the angle between the vectors $\mathbf{r}_1$ and $\mathbf{r}_2$ is smaller than $(1/k_F r)^{1/2}$, where $r$ is the typical length of $\mathbf{r}_1$, $\mathbf{r}_2$.

The above angular restriction constitutes the origin of a zero-bias anomaly in the regime of arcs. Zero-bias anomaly emerges as a result of the suppression of the three-scattering process in the field $h_0$. This suppression is due to curving of the electron trajectory by the angle $\sim r/R_L$ (see Fig. 5), and it occurs when the curving angle exceeds the allowed angle of alignment. Therefore, upon equating $(1/k_F r)^{1/2}$ to $r/R_L$, we find $r=r_{\mathrm{I}}$, which leads us to the conclusion that $\omega\sim v_F/r_{\mathrm{I}}$ is the energy scale at which $\delta\nu(\omega)$ exhibits a feature. Note that in considering the Friedel oscillations, we inferred the scale $r_{\mathrm{I}}$ from a different condition, namely, that the additional phase $\sim(p_0 r_{\mathrm{I}})^3$ due to the *elongation* of a trajectory in magnetic field is $\lesssim 1$. Thus, we conclude that in the regime of

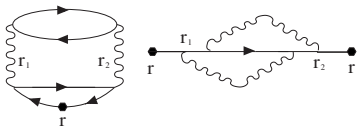


FIG. 7. Diagrams for the second-order corrections Eq. (7.2) (left) and Eq. (7.3) (right) to the density of states.

arcs, the same spatial scale $r_{\mathrm{I}}$ which governs the "dephasing" of $\Pi_{2k_F}(r)$ (a polarization bubble) also governs the suppression of the three-scattering process, which involves *three loops*.

The above analysis of phases in the matrix element of the three-scattering process can be extended to the regime of snakes. This analysis yields that three-scattering process is efficient at distances $r \lesssim r_{\mathrm{II}}$, see Eq. (3.9). Analysis of phases similar to the phase, given by Eq. (6.1), also suggests that *two-scattering* processes are *insensitive* to the magnetic field. This insensitivity can be explained as follows. Calculation of the contribution to the density of states from the three-scattering process with matrix element Eq. (6.1) involves integration over positions of $\mathbf{r}_1$ and $\mathbf{r}_2$, *with respect to the origin*, $\mathbf{r}=0$, which reveals the angular restriction on their orientations. Similar integration for a two-scattering process involves only the orientation of the interaction point $\mathbf{r}$ with respect to the origin. Then, the angular restriction, and its lifting by magnetic field, does not emerge. In the next subsection, the above qualitative arguments are supported by a rigorous calculation.

## VII. DENSITY OF STATES: ANALYTICAL DERIVATION

### A. Absence of a zero-bias anomaly in the second order in the interaction strength

We start from a general expression for the average density of states:

$$\delta\nu(\omega) = -\frac{1}{\pi}\langle \mathrm{Im}\, G_\omega(\mathbf{r},\mathbf{r})\rangle_{h(x,y)}, \tag{7.1}$$

where $\langle\cdots\rangle$ denotes disorder averaging defined by Eq. (5.18). In the second order in interaction strength, the random-field-induced correction to the density of states are determined by two diagrams shown in Fig. 7. The corresponding analytical expressions read

$$\delta\nu_1(\omega) = 4\,\mathrm{Im}\,\frac{2}{\pi}\int\frac{d\Omega}{2\pi}\int d\mathbf{r}d\mathbf{r}_1 d\mathbf{r}_2 G_\omega(\mathbf{r},\mathbf{r}_1)G_\Omega(\mathbf{r}_1,\mathbf{r}_2) \times\{V^2(2k_F)\Pi_{2k_F}(\mathbf{r}_1,\mathbf{r}_2,\omega-\Omega)+V^2(0) \times\Pi_0(\mathbf{r}_1,\mathbf{r}_2,\omega-\Omega)\}G_\omega(\mathbf{r}_2,\mathbf{r}), \tag{7.2}$$

$$\delta\nu_2(\omega) = -2\,\mathrm{Im}\,\frac{2}{\pi}\int\frac{d\Omega}{2\pi}\int d\mathbf{r}d\mathbf{r}_1 d\mathbf{r}_2 G_\omega(\mathbf{r},\mathbf{r}_1) \times G_\Omega(\mathbf{r}_1,\mathbf{r}_2)G_\omega(\mathbf{r}_2,\mathbf{r})\{V(0)[2V(2k_F)-V(0)] \times\Pi_{2k_F}(\mathbf{r}_1,\mathbf{r}_2,\omega-\Omega)+V^2(0)\Pi_0(\mathbf{r}_1,\mathbf{r}_2,\omega-\Omega)\}, \tag{7.3}$$

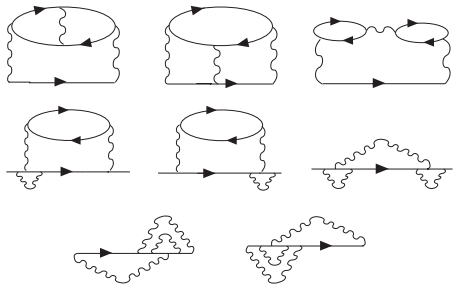

FIG. 8. Third-order diagrams contributing to the zero-bias anomaly in the density of states. The random field enters via the phases of the Green functions.

where $V(0)$ and $V(2k_F)$ are the Fourier components of the interaction potential $V(\mathbf{r})$ with momenta zero and $2k_F$, respectively. Three Green functions in Eqs. (7.2) and (7.3) describe the propagation of electron between the points $(\mathbf{r},\mathbf{r}_1)$, $(\mathbf{r}_1,\mathbf{r}_2)$, and $(\mathbf{r}_2,\mathbf{r})$ (Fig. 7). The polarization bubble describes the creation of electron-hole pair at point $\mathbf{r}_1$ and annihilation at point $\mathbf{r}_2$. The difference in signs in Eqs. (7.2) and (7.3) is due to the fact that the first diagram contains two closed fermionic loops, whereas the second diagram contains only one. Numerical factors 4 and 2 in Eqs. (7.2) and (7.3) come from summation over the spin indices. The difference between them is due the fact the spin of electron-hole pair is not fixed in the first diagram, but it is fixed in the second diagram. The factor of 2 in the product $2V(0)V(2k_F)$ in Eq. (7.3) is related to the annihilation of the electron-hole pair since the hole is annihilated with *initial* electron. Then, the momentum transfer can be $2k_F$ in the course of creation and zero in the course of annihilation, and vice versa.

It is important to emphasize that the Green functions and polarization operators in Eqs. (7.2) and (7.3) contain the information about the random field $h(x,y)$ via their additional phases: $\varphi_{\mathbf{r}_1\to\mathbf{r}_2}$ in $G_\omega(\mathbf{r}_1,\mathbf{r}_2)$ and $2\varphi_{\mathbf{r}_1\to\mathbf{r}_2}$ in $\Pi_{2k_F}(\mathbf{r}_1,\mathbf{r}_2,\omega)$. The phase $\varphi_{\mathbf{r}_1\to\mathbf{r}_2}$ always enters in combination with a main term, $k_F|\mathbf{r}_1-\mathbf{r}_2|$. Obviously, $\Pi_0(\mathbf{r}_1,\mathbf{r}_2,\omega)$ does not contain a field-induced phase. Thus, only the terms containing $\Pi_{2k_F}$ in Eqs. (7.2) and (7.3) should be considered.

Now, it is easy to see that $\delta\nu_1$ and $\delta\nu_2$ *do not* exhibit a field-induced anomaly at small $\omega$. This is because the field dependence is *canceled out* in the integrands of Eqs. (7.2) and (7.3). To see this, we first note that the integration over $\mathbf{r}$ in Eqs. (7.2) and (7.3) can be easily performed using the fact that $\int d\mathbf{r}G_\omega(\mathbf{r}_1,\mathbf{r})G_\omega(\mathbf{r},\mathbf{r}_2)$ is equal to the derivative $\partial G_\omega(\mathbf{r}_1,\mathbf{r}_2)/\partial\omega$. Then, we note that the contribution to $\delta\nu_1$, $\delta\nu_2$ comes only from "slow" terms in the product of two Green functions, $G_\omega(\mathbf{r}_1,\mathbf{r}_2)$, $G_\Omega(\mathbf{r}_1,\mathbf{r}_2)$, and $\Pi_{2k_F}$. These slow terms do not contain rapidly oscillating factors $\exp\{2ik_F|\mathbf{r}_1-\mathbf{r}_2|\}$. On the other hand, cancellation of the rapid terms in the product *automatically* results in the cancellation of the field-dependent terms.

As it was explained in qualitative discussion, the situation changes in the third order in the interactions. The corresponding expression for $\delta\nu(\omega)$ is derived in the next subsection.

### B. General expression for the third-order interaction correction to the density of states

Relevant diagrams for the third-order correction to the density of states are shown in Fig. 8. The same eight diagrams were considered in Ref. 36 in the momentum space. In Ref. 36, the analysis of these diagrams was restricted to small momenta. In our coordinate representation, this means that only $\Pi_0(\mathbf{r})$ parts of the polarization operators was kept, whereas $\Pi_{2k_F}(\mathbf{r})$ parts were neglected. As explained above, to reveal the sensitivity to the random field, we will keep *only* the $\Pi_{2k_F}(\mathbf{r})$ parts. Then, the correction to the Green function corresponding to the sum of the eight diagrams in Fig. 8 acquires the form

$$\delta\nu(\omega) = 2V(0)V(2k_F)[2V(2k_F) - V(0)] \times \mathrm{Im}\,\frac{i}{2\pi^2}\int\frac{d\Omega}{2\pi}\int d\mathbf{r}d\mathbf{r}_1d\mathbf{r}_2 G_\omega(\mathbf{r},\mathbf{r}_1)G_\Omega(\mathbf{r}_1,\mathbf{r}_2) \times \Pi_{2k_F}(\mathbf{r}_1,0,\omega-\Omega)\Pi_{2k_F}(0,\mathbf{r}_2,\omega-\Omega)G_\omega(\mathbf{r}_2,\mathbf{r}). \tag{7.4}$$

All the diagrams reduce to the same integrals. Concerning the difference in numerical coefficients, it comes from the number of closed fermionic loops and the spin degrees of freedom. Taking this into account, interaction coefficient corresponding to the first two diagrams will be $2(-2)^2V^3(2k_F)$. The coefficient of the third diagram is $(-2)^3V^3(2k_F)$. Thus, we see that the contributions $\propto V^3(2k_F)$ cancel each other.

The first and the second diagrams in the second row are equal to each other, and each of them has a coefficient $(-2)^2V(0)V^2(2k_F)$. The coefficient of the last diagram in the second row is $(-2)V^2(0)V(2k_F)$ since it has only one closed fermionic loop. Finally, the first diagram in the third row has only one closed fermionic loop and is equal to the second diagram on the third row. Each of these diagrams contributes with the coefficient $(-2)V(0)V^2(2k_F)$.

On the physical level, the eight diagrams in Fig. 8 describe different electron-electron three-scattering processes. For example, the first diagram corresponds to creation of electron-hole pair by the initial electron followed by rescattering *within a created pair* and, finally, its annihilation. Three stages of this process are illustrated in Fig. 6. However, creation, rescattering, and annihilation of a pair can follow a different scenario, namely, the rescattering process can involve *the initial electron*. This scenario is captured by the second diagram in the first row in Fig. 8.

At this point, we note that the diagrams in Fig. 8 do *not* exhaust all possible three-scattering processes. In fact, all diagrams in Fig. 8 have an identical structure in the sense that they can be combined into a single *generalized* diagram, as shown in Fig. 9(a). There are also eight other diagrams combined into a single generalized diagram, as shown in Fig. 9(b), that are not sensitive to the random field. This is because, in the absence of the random field, the phase factor corresponding to Fig. 9(b) is large, namely, $2[2k_F(r_1+r_2)]$.

The crucial difference between the contributions Eqs. (7.2) and (7.3) and Eq. (7.4) is that the cancellation of the rapid-oscillating terms in the integrand of Eq. (7.4) *preserves*

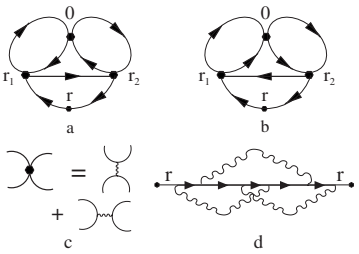


FIG. 9. (a) Eight diagrams for $\delta G_\omega(\mathbf{r},\mathbf{r})$, which are shown in Fig. 8, are combined into one generalized diagram. Electron-electron scattering processes take place at points 0, $\mathbf{r}_1$, and $\mathbf{r}_2$ (b) Eight third-order diagrams that *do not* contribute to the zero-bias anomaly are combined into one generalized diagram. (c) Two types of four-leg interaction vertices are combined into big dots. (d) An example of a third-order diagram of type (b).

the field dependence. To see this, we first replace $\int d\mathbf{r}G_\Omega(\mathbf{r}_1,\mathbf{r})G_\Omega(\mathbf{r},\mathbf{r}_2)$ by $\partial G_\Omega(\mathbf{r}_1,\mathbf{r}_2)/\partial\Omega$, as discussed above, and then consider the phase of the product:

$$G_\Omega(\mathbf{r}_1,\mathbf{r}_2)G_\omega(\mathbf{r}_1,\mathbf{r}_2)\Pi_{2k_F}(0,\mathbf{r}_2,\omega-\Omega)\Pi_{2k_F}(\mathbf{r}_1,0,\omega-\Omega). \tag{7.5}$$

Figure 5(b) illustrates this product graphically. It is seen from Fig. 5(b) that, when the fast oscillating terms $\exp\{2ik_F|\mathbf{r}_1-\mathbf{r}_2|\}$, $\exp\{2ik_Fr_1\}$, and $\exp\{2ik_Fr_2\}$ cancel each other out, the additional phase enters into the product either in combination

$$2\delta\varphi_\Sigma^{(+)} = 2\delta\varphi_{\mathbf{r}_1\to 0} + 2\delta\varphi_{\mathbf{r}_2\to 0} - 2\delta\varphi_{\mathbf{r}_1\to\mathbf{r}_2}, \tag{7.6}$$

or in combination [see Fig. 5(b)]

$$2\delta\varphi_\Sigma^{(-)} = 2\delta\varphi_{\mathbf{r}_1\to 0} - 2\delta\varphi_{\mathbf{r}_2\to 0} + 2\delta\varphi_{\mathbf{r}_1\to\mathbf{r}_2}. \tag{7.7}$$

Since additional phases defined by Eqs. (4.18) and (4.19) are *cubic* in distance, the combinations Eqs. (7.6) and Eq. (7.7) are *nonzero*. This is in contrast to the two-scattering processes, where the cancellation occurs *identically* for arbitrary dependence of $\delta\varphi(r)$ on $r$. In turn, noncancellation of additional phases in Eqs. (7.6) and (7.7) means that the random field causes a zero-bias anomaly, more specifically, a feature in $\delta\nu(\omega)$ at small $\omega$.

The final form of $\delta\nu(\omega)$ emerges upon integration of Eq. (7.4) over azimuthal angles of $\mathbf{r}_1$ and $\mathbf{r}_2$, which can be performed analytically, using the relation

$$\langle e^{i\mathbf{p}(\mathbf{r}_1+\mathbf{r}_2)}\rangle_{\varphi_\mathbf{p},\varphi_{\mathbf{r}_1},\varphi_{\mathbf{r}_2}} = \frac{\sin[p(r_1\pm r_2)+\pi/4]}{p(r_1r_2)^{1/2}}. \tag{7.8}$$

Upon combining rapidly oscillating terms in the integrand of Eq. (7.4) into slow terms, we obtain

$$\delta\nu(\omega) = \delta\nu^{(+)}(\omega) + \delta\nu^{(-)}(\omega), \tag{7.9}$$

where

$$\frac{\delta\nu^{(+)}(\omega)}{\nu_0} = -\frac{(\nu_0 V)^3}{2E_F\pi^{3/2}k_F^{1/2}}\int_{r_2>r_1}\frac{dr_1dr_2}{(r_1r_2)^{3/2}}(r_1+r_2)^{1/2} \times\int_0^\omega d\Omega\,\sin[v_F^{-1}(\omega-\Omega)(r_1+r_2)] \times\sin\left\{2\delta\varphi_\Sigma^{(+)}+\frac{\pi}{4}-\frac{(\omega+\Omega)}{v_F}(r_1+r_2)\right\} \tag{7.10}$$

and

$$\frac{\delta\nu^{(-)}(\omega)}{\nu_0} = -\frac{(\nu_0 V)^3}{2E_F\pi^{3/2}k_F^{1/2}}\int_{r_2>r_1}\frac{dr_1dr_2}{(r_1r_2)^{3/2}}(r_2-r_1)^{1/2} \times\int_0^\omega d\Omega\,\sin[v_F^{-1}(\omega-\Omega)(r_1+r_2)] \times\sin\left\{2\delta\varphi_\Sigma^{(-)}+\frac{\pi}{4}+\frac{(\omega+\Omega)}{v_F}(r_2-r_1)\right\}, \tag{7.11}$$

where we had assumed that the interaction is short ranged and set $V(0)=V(2k_F)=\nu_0 V$. The two contributions in Eq. (7.9) correspond to the locations of the points $\mathbf{r}_1$ and $\mathbf{r}_2$ on the opposite and the same sides from the origin, respectively, see Fig. 5(b).

We note that the phases $\delta\varphi_\Sigma^{(+)}$, $\delta\varphi_\Sigma^{(-)}$, which enter into the argument of sine in Eqs. (7.10) and (7.11), are quadratic in the random field $h(x,y)$, as seen from Eqs. (4.18) and (4.19). This suggests that the averaging over realizations of $h(x,y)$ can be carried out analytically *in the integrands* of Eqs. (7.10) and (7.11). Similarly to the case of Friedel oscillations, it is convenient to perform this averaging separately for regimes I and II. This is done in Secs. VIII and IX below. In the remainder of this section, we will evaluate the interaction correction $\delta\nu(\omega)$ for two particular cases: (i) constant magnetic field $h(x,y)\equiv h_0$ in a clean electron gas and (ii) $h(x,y)\equiv h_0$ in electron gas with a small concentration of pointlike impurities.

### C. Case of constant magnetic field: Oscillations of $\delta\nu(\omega)$

In a constant magnetic field $h(x,y)\equiv h_0$, the characteristic scale of frequency in Eqs. (7.10) and (7.11) is $\omega_0=v_F/r_1$. This was stated in Sec. III. Now, this scale of frequencies emerges naturally upon substituting in Eqs. (7.10) and (7.11) the phases $2\delta\varphi_\Sigma^{(+)}$, $2\delta\varphi_\Sigma^{(+)}$, calculated from Eq. (4.18) in a constant magnetic field:

$$2\delta\varphi_\Sigma^{(\pm)} = \mp\frac{p_0^3}{4}r_1r_2(r_1\pm r_2), \tag{7.12}$$

where $p_0$ is defined by Eq. (3.2). The integrals in Eqs. (7.10) and (7.11) converge at distances $r_1,r_2\sim p_0^{-1}=r_1$. As a result, $\delta\nu^{(+)}$ and $\delta\nu^{(-)}$ are certain universal functions of $\omega r_1/v_F=\omega/\omega_0$. The plot of $\delta\nu^{(+)}+\delta\nu^{(-)}$ vs dimensionless ratio $x=2^{2/3}\omega/\omega_0$ is presented in Fig. 10. To isolate the frequency dependence, in addition to $x$, we had introduced the dimensionless variables $r_1/r_1$ and $r_2/r_1$ after which $\delta\nu(\omega)$ acquires the form

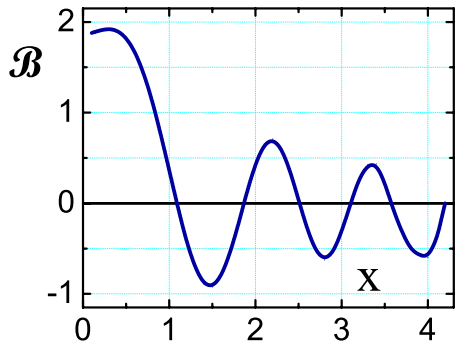


FIG. 10. (Color online) Dimensionless correction Eq. (7.13) to the tunnel density of states in a weak constant magnetic field is plotted vs dimensionless energy $x=2^{2/3}\omega/\omega_0$. The plot is obtained upon numerical integration in Eqs. (7.10) and (7.11).

$$\frac{\delta\nu(\omega)}{\nu_0} = -\frac{(\nu_0 V)^3}{2^{2/3}(\pi k_F r_1)^{3/2}}\mathcal{B}(x). \tag{7.13}$$

The integral over $\Omega$ in Eqs. (7.10) and (7.11) can be evaluated analytically. The remaining dimensionless double integrals were calculated numerically. While the characteristic scale, $x\sim 1$, of change of the function $\mathcal{B}(x)$ follows from qualitative consideration, Fig. 10 indicates that $\mathcal{B}(x)$ also exhibits sizable oscillations. These oscillations come only from the contribution $\delta\nu^{(+)}$. They owe their existence to the peculiar structure of the argument of sine in Eq. (7.10). Namely, this argument has saddle points with respect to *both* $r_1$ and $r_2$ at $r_1=r_2=2^{1/3}r_1(\omega/\omega_0)^{1/2}/3^{1/2}$. Oscillatory behavior of $\mathcal{B}(x)$ is governed by the value of the argument at the saddle point, which is $\sim(\omega/\omega_0)^{3/2}$. Strictly speaking, the saddle point determines the value of the integral only when $\omega\gg\omega_0$. However, numerics shows that oscillations in Fig. 10 set in starting already from $x\sim 1$. These oscillations reflect the distinguished contribution from the three-scattering process, shown in Fig. 5(b), in which scattering events occur at $r_1=r_2=2^{1/3}r_1(\omega/\omega_0)^{1/2}/3^{1/2}$.

Equation (7.13) and Fig. 10 constitute an experimentally verifiable prediction. Correction Eq. (7.13) describes the feature in the tunneling conductance of a clean two-dimensional electron gas as a function of bias that emerges in a weak magnetic field $h_0$. It follows from the prefactor in Eq. (7.13) that the magnitude of $\delta\nu$ scales with $h_0$ as $r_1^{-3/2}\propto h_0$. We emphasize that the correction $\delta\nu(\omega)$ remains distinguishable even when the structure in the density of states due to the Landau quantization is completely smeared out, e.g., due to finite temperature. This follows from the above relation between $\omega_0$ and the cyclotron frequency $\omega_c$, namely, $(\omega_c/\omega_0)\sim(\omega_c/E_F)^{1/3}\ll 1$.

In discussing the relevance to the experiment, one should have in mind that realistic samples always contain a certain degree of disorder. Therefore, the question remains as to whether the oscillations of $\delta\nu(\omega)$ in a constant magnetic field survive in the presence of the short-range impurities. This question is nontrivial since impurities themselves give rise to

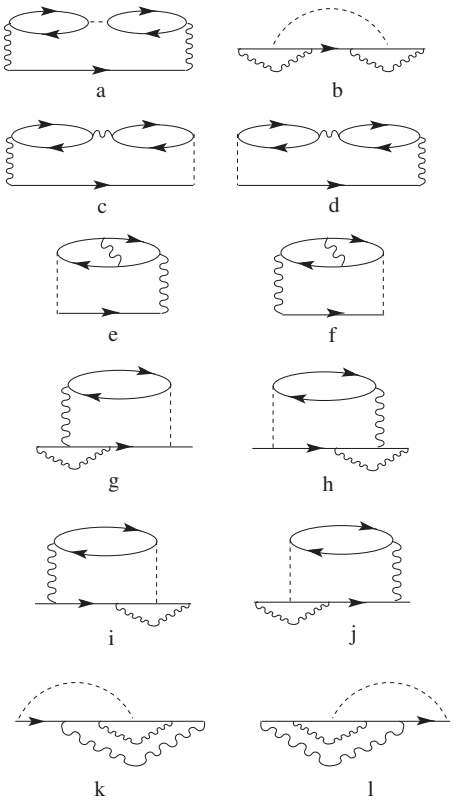


FIG. 11. Second-order diagrams contributing to the oscillating part (see Fig. 4) of the ballistic zero-bias anomaly in a weak constant magnetic field. The magnetic field enters through the phases Eq. (4.7) of the Green functions. The dashed line represents the impurity scattering. All 12 diagrams (a)–(l) contain two static polarization operators.

the singular correction to $\delta\nu(\omega)$ (zero-bias anomaly) even in a zero field. Then, the above question can be reformulated as follows: whether the field-induced oscillations are distinguishable on the background of a zero-bias anomaly. It turns out that by introducing the Friedel oscillations, pointlike impurities actually enhance the oscillatory part of $\delta\nu(\omega)$. This question is addressed in the next subsection.

### D. Ballistic zero-bias anomaly in a constant magnetic field

Conventional ballistic zero-bias anomaly[3] caused by pointlike impurities is described by two second-order diagrams, shown Fig. 7, in which one of two interaction lines is replaced by an impurity line. As was shown in Ref. 3, these diagrams with one interaction line and one impurity line yield a singular correction $\delta\nu(\omega)/\nu_0 \sim (\nu_0 V/E_F\tau)\ln(\omega)$ to the density of states. Here, $\tau^{-1}$ is the scattering rate proportional to the impurity concentration. Qualitatively, the singular correction originates from the combined scattering of electron by the impurity and the Friedel oscillation $\propto \sin(2k_F r)/r^2$, created *by the same impurity*. This Friedel oscillation is represented by the polarization loop in Fig. 7. In the presence of the impurity, this loop describes *static* response of the electron gas, and thus the polarization operator $\Pi_{2k_F}(\omega, r)$ corresponding to the loop should be taken at $\omega=0$. As was mentioned in Sec. III, a weak perpendicular magnetic field $h$ leaves the logarithmic correction unchanged. To reveal the sensitivity to $h$, one should calculate $\delta\nu$ to the next (second) order in $V$. Corresponding diagrams with one impurity and two interaction lines are shown in Figs. 11–13. It is easy to see that there are overall 24 different diagrams. Indeed, the generalized diagram, Fig. 9(a), for the third-order *interaction* correction contains three generalized four-leg vertices shown in Fig. 9(c). Hence, Fig. 9(a) represents $2^3=8$ different diagrams. In each of these eight diagrams, the impurity line can replace the interaction line in three places, generating one of the 24 different diagrams that are shown in Figs. 11–13. All these diagrams are divided into three groups according to their dependence on $\omega$. Namely, *all* 12 diagrams in Fig. 11 have the same $\omega$ dependence. Similarly, the $\omega$ dependence of *all* eight diagrams in Fig. 12 is the same. This also applies to the four diagrams in Fig. 13. However, the corresponding $\omega$ dependencies are slightly different from each other. The origin of this difference can be traced from comparison of the diagrams in Figs. 11(a), 12(a), and 13(b). The diagram in Fig. 11(a) contains two polarization loops separated by the impurity line. As a result, the expression corresponding to this diagram contains two static polarization operators

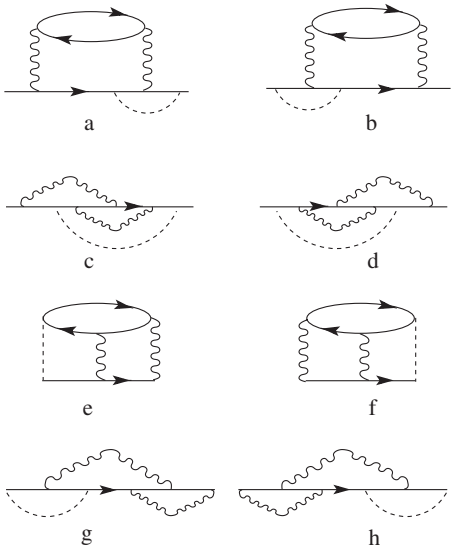


FIG. 12. 8 out of the total 24 second-order diagrams for ballistic zero-bias anomaly in a weak constant magnetic field, which contain one dynamic polarization operator.

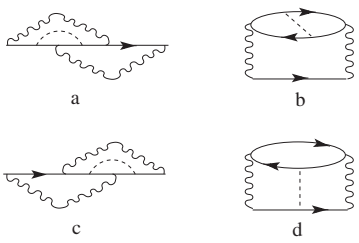


FIG. 13. 4 out of the total 24 second-order diagrams for the ballistic zero-bias anomaly in a weak constant magnetic field, which contain a polarization loop crossed by the impurity line.

$\Pi_{2k_F}(0,r)$. The diagram in Fig. 12(a) contains *one* finite-$\omega$ polarization loop $\Pi_{2k_F}(\omega,r)$. Finally, the diagram in Fig. 13(b) does not contain polarization operators at all but rather a different object, namely, a polarization loop *crossed* by the impurity line. Important is that the expression corresponding to this object:

$$\prod(\omega-\Omega,|\mathbf{r}_1-\mathbf{r}_2|)=-i\int\frac{d\Omega_1}{2\pi}G_{\Omega_1}(0,\mathbf{r}_1)G_{\omega-\Omega+\Omega_1}(\mathbf{r}_1,0)\times G_{\omega-\Omega+\Omega_1}(0,\mathbf{r}_2)G_{\Omega_1}(\mathbf{r}_2,0), \quad (7.14)$$

contains a "fast" part, $\Pi_{2k_F}(\omega,r)$, which oscillates as $\exp(2ik_F|\mathbf{r}_1-\mathbf{r}_2|)$, i.e., in the same way as a polarization operator.

The full analytical expression corresponding to the diagram in Fig. 11(a) reads

$$\begin{aligned}\delta\nu_1(\omega,h)&=\mathrm{Im}\,\frac{4V^2(2k_F)}{2\pi^2\nu_0\tau}\int d\mathbf{r}d\mathbf{r}_1d\mathbf{r}_2G_\omega(\mathbf{r},\mathbf{r}_1)G_\omega(\mathbf{r}_1,\mathbf{r}_2)\times\Pi_{2k_F}(0,\mathbf{r}_1)\Pi_{2k_F}(0,\mathbf{r}_2)G_\omega(\mathbf{r}_2,\mathbf{r})\\&=\mathrm{Im}\,\frac{6V^2(2k_F)}{\pi^2\nu_0\tau}\int d\mathbf{r}_1d\mathbf{r}_2\partial_\omega G_\omega(\mathbf{r}_1,\mathbf{r}_2)G_\omega(\mathbf{r}_1,\mathbf{r}_2)\times\Pi_{2k_F}(0,\mathbf{r}_1)\Pi_{2k_F}(0,\mathbf{r}_2), \quad (7.15)\end{aligned}$$

where in the second identity, we had performed integration over $\mathbf{r}$.

The analytical expression for the diagram in Fig. 12(a) has the form

$$\begin{aligned}\delta\nu_2(\omega,h)&=-\mathrm{Im}\,\frac{2V^2(2k_F)}{2\pi^2\nu_0\tau}\times\int d\mathbf{r}d\mathbf{r}_1d\mathbf{r}_2G_\omega(\mathbf{r},\mathbf{r}_1)G_\omega(\mathbf{r}_1,0)G_\omega(\mathbf{r}_2,\mathbf{r})\\&\times\int\frac{d\Omega}{2\pi}G_\Omega(0,\mathbf{r}_1)G_\Omega(\mathbf{r}_1,\mathbf{r}_2)\Pi_{2k_F}(\omega-\Omega,|\mathbf{r}_1-\mathbf{r}_2|). \quad (7.16)\end{aligned}$$

Finally, the expression for the diagram in Fig. 13(b) is the following:

$$\begin{aligned}\delta\nu_3(\omega,h)&=-\mathrm{Im}\,\frac{2V^2(2k_F)}{2\pi^2\nu_0\tau}\times\int d\mathbf{r}d\mathbf{r}_1d\mathbf{r}_2G_\omega(\mathbf{r},\mathbf{r}_1)G_\omega(\mathbf{r}_2,\mathbf{r})\\&\times\int\frac{d\Omega}{2\pi}\int\frac{d\Omega_1}{2\pi}G_\Omega(\mathbf{r}_1,\mathbf{r}_2)G_{\Omega_1}(0,\mathbf{r}_1)G_{\omega-\Omega+\Omega_1}\times(\mathbf{r}_1,0)G_{\omega-\Omega+\Omega_1}(0,\mathbf{r}_2)G_{\Omega_1}(\mathbf{r}_2,0). \quad (7.17)\end{aligned}$$

Upon integration over $\mathbf{r}$, it can be expressed through $\Pi_{2k_F}(r)$, defined by Eq. (7.14), as

$$\begin{aligned}\delta\nu_3(\omega,h)&=-\frac{V^2(2k_F)}{\pi^4\nu_0\tau}\times\int d\mathbf{r}_1d\mathbf{r}_2\partial_\omega\,\mathrm{Im}\,G_\omega(\mathbf{r}_1,\mathbf{r}_2)\int_0^\omega\frac{d\Omega}{2\pi}\times\mathrm{Im}\,G_\Omega(\mathbf{r}_1,\mathbf{r}_2)\mathrm{Im}\prod{}_{2k_F}(\omega-\Omega,|\mathbf{r}_1-\mathbf{r}_2|). \quad (7.18)\end{aligned}$$

Despite that all 12 diagrams in Fig. 11 have the same frequency dependence, their prefactors represent different combinations of $V^2(2k_F)$, $V^2(0)$, and $V(2k_F)V(0)$. The same applies to the eight diagrams in Fig. 12 and to the four diagrams in Fig. 13. Taking into account the numerical factors in these combinations amounts to the following replacements: in $\delta\nu_1$,

$$4V^2(2k_F)\to 3V^2(0), \quad (7.19)$$

in $\delta\nu_2$,

$$-2V^2(2k_F)\to 4[V(0)V(2k_F)-V^2(2k_F)-V^2(0)], \quad (7.20)$$

and in $\delta\nu_3$,

$$-2V^2(2k_F)\to 2[V(0)V(2k_F)-V^2(2k_F)-V^2(0)]. \quad (7.21)$$

These replacements must be taken into account when calculating the full correction $\delta\nu(\omega)$ from $\delta\nu_1$, $\delta\nu_2$, and $\delta\nu_3$.

Below, we demonstrate that all three contributions $\delta\nu_1$, $\delta\nu_2$, and $\delta\nu_3$ are oscillatory functions of $\omega$. Detailed derivation will be presented only for $\delta\nu_1$.

Analogously to the derivation of Eqs. (7.10) and (7.11), we can perform the integration over the azimuthal angles of $\mathbf{r}_1$ and $\mathbf{r}_2$ analytically using Eq. (7.8). Then, extracting a slow term from the product of trigonometrical functions, we obtain $\delta\nu_1(\omega)=[6\nu_0^3V^2(2k_F)/E_F\tau](\omega_0/E_F)^{1/2}P_1(2^{2/3}\omega/\omega_0)$, with $\omega_0=2^{1/3}\omega_c^{2/3}E_F^{1/3}$, where the function $P_1(x)$ is defined as

$$P_1(x)=P_1^+(x)+P_1^-(x), \quad (7.22)$$

where

$$P_1^+(x)=\sigma\int_{\rho_2>\rho_1}\frac{d\rho_1d\rho_2}{(\rho_1\rho_2)^{3/2}}\left\{(\rho_1+\rho_2)^{1/2}\left\{\cos\left[x(\rho_1+\rho_2)-\frac{\pi}{4}-\rho_1\rho_2(\rho_1+\rho_2)\right]-\cos\left[x(\rho_1+\rho_2)-\frac{\pi}{4}\right]\right\}\right\}, \quad (7.23)$$

$$P_1^-(x)=-\sigma\int_{\rho_2>\rho_1}\frac{d\rho_1d\rho_2}{(\rho_1\rho_2)^{3/2}}\left\{(\rho_2-\rho_1)^{1/2}\left\{\cos\left[x(\rho_2-\rho_1)+\frac{\pi}{4}+\rho_1\rho_2(\rho_2-\rho_1)\right]-\cos\left[x(\rho_2-\rho_1)+\frac{\pi}{4}\right]\right\}\right\}. \quad (7.24)$$

Here, the constant factor $\sigma$ is given by $\sigma=[3(2^{1/6})]/\pi^{3/2}$. In Appendix E, we demonstrate how the function $P_1(x)$ can be cast in the form that is convenient for numerical evaluation

and extracting asymptotes. This form is given by the following double integral:

$$P_1(x) = 4\sigma \int_0^\infty \frac{dz}{z^{3/2}} \int_{-4}^0 \frac{dv}{\sqrt{v+4}} \times \left( \cos\left[ xz + \frac{\pi}{4} + \frac{z^3}{v} \right] - \cos\left[ xz + \frac{\pi}{4} \right] \right). \tag{7.25}$$

The fact that $P_1(x)$ oscillates at large $x \gg 1$ follows from the observations that (i) the first cosine in the brackets in Eq. (7.25) has a saddle point $z=(x|v|/3)^{1/2}$ and (ii) the major contribution to the integral over $v$ comes from the lower limit $v=-4$ (corresponding steps are outlined in Appendix D). This yields

$$P_1(x)|_{x\gg 1} = \frac{2^{5/3}3^{9/4}}{\pi^{1/2}} \frac{1}{x^{7/4}} \sin\left[ 4\left(\frac{x}{3}\right)^{3/2} + \frac{\pi}{4} \right]. \tag{7.26}$$

The argument $x^{3/2}$ in the cosine in Eq. (7.26) can be presented as $\omega^{3/2}/(2^{1/2}\omega_c E_F^{1/2})$, so that the period in $\omega$ is much bigger than the cyclotron energy $\omega_c$, as was discussed above.

The analysis of the contributions $\delta\nu_2(\omega)$ and $\delta\nu_3(\omega)$ can be carried out in a similar way. They exhibit the same oscillations as Eq. (7.26). The difference is that, due to integration over $\Omega$ in Eqs. (7.16) and (7.18), both $\delta\nu_2(\omega)$ and $\delta\nu_3(\omega)$ contain an extra factor $\omega/\omega_0$, see Eq. (3.13), and thus their contribution to the net correction $\delta\nu$ is dominant at $\omega \gg \omega_0$.

## VIII. ZERO-BIAS ANOMALY IN THE AVERAGED DENSITY OF STATES IN REGIME I

With the help of the identity Eq. (5.5), the integrand in the average $\delta\nu(\omega)$ can be expressed in terms of functions $U_{1,2}[r_1 r_2 (r_2 \pm r_1) p_0^3/4]$, where the functions $U_{1,2}$ are defined as

$$U_1(x) = \left(\frac{\pi}{2}\right)^{1/2} \sqrt{\frac{(1+x^2)^{1/2}+1}{1+x^2}}, \tag{8.1}$$

$$U_2(x) = \left(\frac{\pi}{2}\right)^{1/2} \sqrt{\frac{(1+x^2)^{1/2}-1}{1+x^2}}. \tag{8.2}$$

Upon introducing dimensionless variables $\rho_{1,2} = p_0 r_{1,2}/2^{2/3}$, we present the final result in the form

$$\frac{\delta\nu(\omega)}{\nu_0} = \mathcal{C}\mathcal{I}\left(\frac{\omega}{\omega_0}\right), \tag{8.3}$$

with

$$\omega_0 = v_F p_0 = 2E_F \left(\frac{h_0}{k_F^2 \Phi_0}\right)^{2/3}, \tag{8.4}$$

and with constant $\mathcal{C}$ defined as

$$\mathcal{C} = -\frac{(\nu_0 V)^3}{2\pi}\left(\frac{h_0}{k_F^2\Phi_0}\right) = -\frac{(\nu_0 V)^3}{4\sqrt{2}\pi}\left(\frac{\omega_0}{E_F}\right)^{3/2}. \tag{8.5}$$

The dimensionless function $\mathcal{I}(z)$ describing the shape of the anomaly is given by the following double integral over $\rho_1$, $\rho_2$:

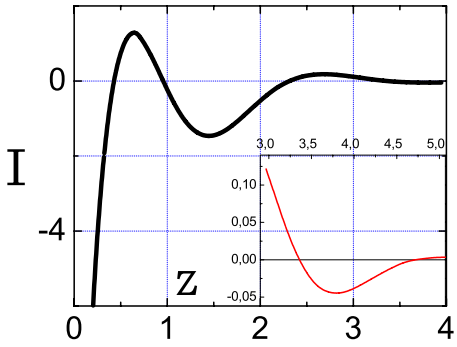


FIG. 14. (Color online) Dimensionless function $\mathcal{I}(z)$ describing the shape of a zero-bias anomaly in regime I is plotted from Eq. (8.6) versus dimensionless energy, $z=\omega/\omega_0$. Inset in the lower-right corner: enlarged plot of $\mathcal{I}(z)$ in the domain $3<z<5$.

$$\mathcal{I}(z) = \mathcal{I}^+(z) + \mathcal{I}^-(z) = \int_{\rho_2>\rho_1} \frac{d\rho_1 d\rho_2}{(\rho_1\rho_2)^{3/2}} \int_0^z dz' \sin[(z-z') \times (\rho_1+\rho_2)]\{S_+(\rho_1,\rho_2) + C_+(\rho_1,\rho_2) + S_-(\rho_1,\rho_2) + C_-(\rho_1,\rho_2)\}, \tag{8.6}$$

where the functions $S_+$, $S_-$, $C_+$, and $C_-$ are defined as

$$S_\pm(\rho_1,\rho_2) = (\rho_1 \pm \rho_2)^{1/2} \sin\left[\frac{\pi}{4} \mp (z+z')(\rho_1 \pm \rho_2)\right] \times \{U_1[\rho_1\rho_2(\rho_1 \pm \rho_2)] - \sqrt{\pi}\}, \tag{8.7}$$

$$C_\pm(\rho_1,\rho_2) = (\rho_1 \pm \rho_2)^{1/2} \cos\left[\frac{\pi}{4} \mp (z+z') \times (\rho_1 \pm \rho_2)\right] U_2[\rho_1\rho_2(\rho_1 \mp \rho_2)]. \tag{8.8}$$

In the definitions of $S_+$ and $S_-$, we had subtracted from the function $U_1(\alpha)$ the zero-field value $U_1(0)=\sqrt{\pi}$. Integration over $z'$ in Eq. (8.6) can be easily carried out analytically. The remaining integrals over $\rho_1$, $\rho_2$ were evaluated numerically. Direct numerical integration encounters difficulties due to very fast oscillations of the integrand in Eq. (8.6). These difficulties can be overcome by a proper change of variables in the integrand. This procedure is described in Appendix D. The resulting shape of the zero-bias anomaly is shown in Fig. 14. The small-$z \ll 1$ behavior of $\mathcal{I}(z)$ is $8 \ln z$, i.e., it diverges logarithmically. The cutoff is chosen from the condition that $\mathcal{I}(z)$ approaches zero at large $z$. Note that $\mathcal{I}(z)$ exhibits a pronounced feature around $z=1$. The origin of this feature lies in strong oscillations of the integrand in Eq. (7.9). The "trace" of these oscillations *survives* after averaging over the magnitude of the random field. In fact, the oscillations persist beyond $z=3$. This is reflected in the $z \gg 1$ asymptote of the function $\mathcal{I}(z)$,

$$\mathcal{I}^+(z)|_{z\gg 1} \approx -2^{3/4}\sqrt{\pi}\frac{\sin(2^{8/3}\sqrt{3}z)}{z^{3/4}} \exp\{-2^{8/3}z\}. \tag{8.9}$$

To derive this asymptote, it is more convenient to first take the limit of large $\omega$ in Eq. (7.9) and perform the averaging

over the random field only *as a last step*. In the limit $\omega \gg \omega_0$, the following simplifications of Eq. (7.9) become possible. Firstly, the second term in the square brackets can be neglected, since it does not produce oscillatory contribution to $\delta\nu$. Secondly, one can set $\Omega=0$ in the integrand, so that the integration over $\Omega$ reduces to multiplying by $\omega$. Lastly, upon converting the product of sines into the difference of cosines, one finds that the $\omega$ dependence is present only in the term corresponding to the difference of arguments. As a result, the oscillatory part of $\delta\nu(\omega)$ at $\omega \gg \omega_0$ acquires the form

$$\left\langle \frac{\delta\nu(\omega)}{\nu_0} \right\rangle = -\frac{(\nu_0 V)^3 \omega \omega_0^{1/2}}{2^{15/6}\pi^{3/2}E_F^{3/2}} \int_{\rho_2>\rho_1} \frac{d\rho_1 d\rho_2}{(\rho_1\rho_2)^{3/2}}(\rho_1+\rho_2)^{1/2} \times \left\langle \left(\frac{h}{h_0}\right)\cos\left[\rho_1\rho_2(\rho_1+\rho_2)+\frac{\pi}{4} - \frac{2^{5/3}\omega}{\omega_0}\left(\frac{h_0}{h}\right)^{2/3}(\rho_1+\rho_2)\right]\right\rangle_{h(x,y)}. \quad (8.10)$$

The steps leading from this expression to the asymptote Eq. (8.9) are outlined in Appendix E.

## IX. ZERO-BIAS ANOMALY IN AVERAGED DENSITY OF STATES IN REGIME II

### A. Three polarization operators: Averaging of the net magnetic phase factor over realizations of random magnetic field

To derive analytical expressions for $\delta\nu^{(+)}(\omega)$ and $\delta\nu^{(-)}(\omega)$, one has to perform averaging of Eqs. (7.10) and (7.11) over realizations of the random field. Such an averaging has already been carried out for the Friedel oscillations. In the latter case, we had averaged $\langle\exp(2i\delta\varphi_{0\to\mathbf{r}})\rangle$. In the case of the density of states, the exponents to be averaged are $\langle\exp(2i\delta\varphi_\Sigma^{(\pm)})\rangle$, defined by Eqs. (7.6) and (7.7). Our most important observation is that the *net* phase $\delta\varphi_\Sigma^{(-)}=\delta\varphi_{0\to\mathbf{r}_1}+\delta\varphi_{\mathbf{r}_1\to\mathbf{r}_2}+\delta\varphi_{\mathbf{r}_2\to 0}$ *does not* contain integrals of $\Lambda^2(x)$ since they cancel out. This can be clearly seen from Eq. (4.17). Instead, $\delta\varphi_\Sigma^{(-)}$ is expressed via integrals of $\Lambda(x)$ *in the first power* as follows:

$$\delta\varphi_\Sigma^{(-)} = \frac{1}{\Phi_0^2 k_F}\left[\frac{1}{r_1}\left(\int_0^{r_1} dx\Lambda(x)\right)^2 + \frac{1}{r_2-r_1}\left(\int_{r_1}^{r_2} dx\Lambda(x)\right)^2 - \frac{1}{r_2}\left(\int_0^{r_2} dx\Lambda(x)\right)^2\right]. \quad (9.1)$$

This cancellation, as we demonstrate below, has a dramatic consequence for the average $\langle\exp(i\delta\varphi_\Sigma)\rangle$. It turns out that while $\langle\exp(i\delta\varphi_{0\to\mathbf{r}})\rangle$ decays with $r$ *exponentially*, the average $\langle\exp(i\delta\varphi_\Sigma)\rangle$ falls off only as $a$ power law. This, in turn, leads to a slow decay of a zero-bias anomaly, $\delta\nu(\omega/\omega_1)$, with $\omega$.

On the technical level, cancellation of $\int dx\Lambda^2(x)$ terms leads to a drastic simplification of the disorder averaging of Eqs. (7.10) and (7.11) in regime II, as compared to the averaging of the Friedel oscillations in Sec. V B, since the averaging of $\exp(2i\delta\varphi_\Sigma)$ can be performed with the help of the Hubbard–Stratonovich transformation. For the purpose of functional averaging, it is convenient to rewrite Eq. (9.1) in a slightly different form:

$$\delta\varphi_\Sigma^{(-)} = \frac{1}{\Phi_0^2 k_F(r_2-r_1)}\left[\sqrt{\frac{r_2}{r_1}}\int_0^{r_1} dx\Lambda(x) - \sqrt{\frac{r_1}{r_2}}\int_0^{r_2} dx\Lambda(x)\right]^2. \quad (9.2)$$

Subsequent integration by parts yields the further simplification of Eq. (9.2):

$$\delta\varphi_\Sigma^{(-)} = \frac{1}{\Phi_0^2 k_F(r_2-r_1)}\left[\sqrt{\frac{r_2}{r_1}}\int_0^{r_1} dx(r_1-x)h(x,0) - \sqrt{\frac{r_1}{r_2}}\int_0^{r_2} dx(r_2-x)h(x,0)\right]^2. \quad (9.3)$$

Now, the averaging over realizations of $h(x,y)$ can be performed by a sequence of standard steps outlined below.

#### 1. AVERAGING PROCEDURE

Using Eq. (9.1), we rewrite the definition of average $\langle\exp(2i\delta\varphi_\Sigma)\rangle$ by introducing the auxiliary integration variable $c$:

$$\langle\exp\{2i\delta\varphi_\Sigma^{(-)}\}\rangle = \int_{-\infty}^{\infty} dc\,\exp(-ic^2)\left\langle \delta\left(c - \frac{\sqrt{2}}{\Phi_0 k_F^{1/2}\sqrt{r_2-r_1}} \times\left[\sqrt{\frac{r_2}{r_1}}\int_0^{r_1} dx(r_1-x)h(x,0) - \sqrt{\frac{r_1}{r_2}}\int_0^{r_2} dx(r_2-x)h(x,0)\right]\right)\right\rangle_{h(x,y)}, \quad (9.4)$$

where the averaging $\langle\cdots\rangle_{h(x,y)}$ is defined by Eq. (5.18). Next, we use the following integral representation of the $\delta$ function in Eq. (9.4)

$$\langle\exp\{2i\delta\varphi_\Sigma^{(-)}\}\rangle = \int_{-\infty}^{\infty} dc\,\exp(-ic^2)\int_{-\infty}^{\infty}\frac{dt}{2\pi}e^{ict}\left\langle \exp\left\{-it\sqrt{2}\left[\sqrt{\frac{r_2}{r_1}}\int_0^{r_1}\frac{dx(r_1-x)h(x,0)}{\Phi_0 k_F\sqrt{r_2-r_1}} - \sqrt{\frac{r_1}{r_2}}\int_0^{r_2}\frac{dx(r_2-x)h(x,0)}{\Phi_0 k_F\sqrt{r_2-r_1}}\right]\right\}\right\rangle_{h(x,y)}. \quad (9.5)$$

Now, the integration over $c$ can be performed explicitly, yielding

$$\langle \exp\{2i\delta\varphi_\Sigma^{(-)}\}\rangle = \sqrt{\frac{\pi}{2}} e^{-i\pi/4} \int_{-\infty}^{\infty} \frac{dt}{2\pi} e^{it^2/4} \times \left\langle \exp\left\{ -it\sqrt{2}\left[ \sqrt{\frac{r_2}{r_1}} \int_0^{r_1} \frac{dx(r_1-x)h(x,0)}{\Phi_0 k_F \sqrt{r_2-r_1}} - \sqrt{\frac{r_1}{r_2}} \int_0^{r_2} \frac{dx(r_2-x)h(x,0)}{\Phi_0 k_F \sqrt{r_2-r_1}} \right] \right\} \right\rangle_{h(x,y)}. \tag{9.6}$$

It follows from Eq. (9.6) that the evaluation of $\langle \exp\{2i\delta\varphi_\Sigma^{(-)}\}\rangle$ reduces to the Gaussian averaging of the exponent of a *linear* in $h(x)$ functional, which is standard:

$$\left\langle \exp\left\{ -it \int_0^{r_2} dx \int_{-\infty}^{\infty} dy h(x,y) f(x) \delta(y) \right\} \right\rangle_{h(x,y)} = \exp\left\{ -\frac{t^2}{4} \int_0^{r_2} dx_1 \int_0^{r_2} dx_2 f(x_1) K(x_1,0,x_2,0) f(x_2) \right\}, \tag{9.7}$$

where $K(x_1,0,x_2,0)$ is related to the correlator of the random field Eq. (2.1) as $K(x_1,0,x_2,0)=h_0^2 \mathrm{K}(|x_1-x_2|/\xi)$. Subsequent integration over $t$ yields the final result

$$\langle \exp\{2i\delta\varphi_\Sigma^{(-)}\}\rangle = \frac{1}{\sqrt{1+i\int_0^{r_2}\int_0^{r_2} dx_1 dx_2 f(x_1) K(x_1,0,x_2,0) f(x_2)}}. \tag{9.8}$$

As seen from Eq. (9.6), the function $f(x)$ in Eq. (9.7) has the form

$$f_-(x) = \frac{\sqrt{2}}{\Phi_0 k_F^{1/2} \sqrt{r_2-r_1}} \left[ \sqrt{\frac{r_2}{r_1}} (r_1-x)\theta(r_1-x) - \sqrt{\frac{r_1}{r_2}} (r_2-x) \right]. \tag{9.9}$$

Averaging of $\exp\{i\delta\varphi_\Sigma^{(+)}\}$ is performed similarly and also yields Eq. (9.7) with $f(x)$ having the form

$$f_+(x) = \frac{\sqrt{2}}{\Phi_0 k_F^{1/2} \sqrt{r_2}} \left[ \sqrt{\frac{r_1+r_2}{r_1}} (r_1-x)\theta(r_1-x) - \sqrt{\frac{r_1}{r_1+r_2}} (r_1+r_2-x) \right]. \tag{9.10}$$

We emphasize that expression Eq. (9.8) is *general* and is valid for arbitrary $h_0$ and $\xi$, i.e., in both regimes I and II. For regime I, we had already performed the averaging over realizations of the random field. With regard to Eq. (9.8), regime I corresponds to replacement of the correlator *by unity*. In regime II, the distances $r_1, r_2$ are much larger than $\xi$. For this reason, in regime II, the correlator in Eq. (9.8) can be replaced by $\sqrt{2}\pi\gamma\xi\delta(x_1-x_2)$, with $\gamma$ defined by Eq. (5.22). Then the averages $\langle \exp\{2i\delta\varphi_\Sigma^{(-)}\}\rangle$ and $\langle \exp\{2i\delta\varphi_\Sigma^{(+)}\}\rangle$ can be expressed in terms of dimensionless ratios

$$\varrho_1 = \frac{r_1}{\sqrt{6} r_{\mathrm{II}}}, \quad \varrho_2 = \frac{r_2}{\sqrt{6} r_{\mathrm{II}}}, \tag{9.11}$$

where the characteristic length $r_{\mathrm{II}}$ is defined by Eq. (5.29).

Equation (9.8) and analogous expression for $\langle \exp\{2i\delta\varphi_\Sigma^{(+)}\}\rangle$ are sufficient to perform the averaging over realizations of random magnetic field in Eqs. (7.10) and (7.11). However, averaged Eqs. (7.10) and (7.11) contain the real and imaginary parts:

$$\langle \exp\{2i\delta\varphi_\Sigma^{(\pm)}\}\rangle = \mathcal{U}_1^{\pm}(\varrho_1,\varrho_2) + i\mathcal{U}_2^{\pm}(\varrho_1,\varrho_2), \tag{9.12}$$

of the average exponents *separately*. The expressions for $\mathcal{U}_1^{\pm}$ and $\mathcal{U}_2^{\pm}$ readily follow after replacing the correlator by the delta function and performing integrations over $x_1$ and $x_2$ in Eq. (9.8):

$$\mathcal{U}_1^- = \frac{\sqrt{\sqrt{\varrho_1^2(\varrho_2-\varrho_1)^2+1}+1} + \sqrt{\sqrt{\varrho_1^2(\varrho_2-\varrho_1)^2+1}-1}}{\sqrt{2}\sqrt{\varrho_1^2(\varrho_2-\varrho_1)^2+1}}, \tag{9.13}$$

$$\mathcal{U}_2^- = \frac{\sqrt{\sqrt{\varrho_1^2(\varrho_2-\varrho_1)^2+1}+1} - \sqrt{\sqrt{\varrho_1^2(\varrho_2-\varrho_1)^2+1}-1}}{\sqrt{2}\sqrt{\varrho_1^2(\varrho_2-\varrho_1)^2+1}}, \tag{9.14}$$

$$\mathcal{U}_1^+ = \frac{\sqrt{\sqrt{\varrho_1^2\varrho_2^2+1}+1} + \sqrt{\sqrt{\varrho_1^2\varrho_2^2+1}-1}}{\sqrt{2}\sqrt{\varrho_1^2\varrho_2^2+1}}, \tag{9.15}$$

$$\mathcal{U}_2^+ = \frac{\sqrt{\sqrt{\varrho_1^2\varrho_2^2+1}+1} - \sqrt{\sqrt{\varrho_1^2\varrho_2^2+1}-1}}{\sqrt{2}\sqrt{\varrho_1^2\varrho_2^2+1}}. \tag{9.16}$$

Final expressions for the contributions $\langle \delta\nu^-(\omega)\rangle$ and $\langle \delta\nu^+(\omega)\rangle$ to the averaged density of states in the second regime are obtained by performing integration over $\Omega$ in Eqs. (7.10) and (7.11) and using Eqs. (9.13)–(9.16). We present this expression in the form similar to Eq. (8.3):

$$\left\langle \frac{\delta\nu^{\pm}(\omega)}{\nu_0} \right\rangle = \mathcal{D}\mathcal{J}^{\pm}\left(\frac{\omega}{\omega_1}\right), \tag{9.17}$$

where the prefactor $\mathcal{D}$ is defined as

$$\mathcal{D} = -\frac{(\nu_0 V)^3}{6^{3/4}(\pi k_F r_{\mathrm{II}})^{3/2}}, \tag{9.18}$$

and the dimensionless functions $\mathcal{J}^{\pm}$ are the following integrals over $\varrho_1$, $\varrho_2$:

$$\mathcal{J}_1(z) = \frac{1}{4}\int_{\varrho_2>\varrho_1} \frac{d\varrho_1 d\varrho_2}{(\varrho_1\varrho_2)^{3/2}} (\varrho_2-\varrho_1)^{1/2}[\mathcal{U}_1^-(\varrho_1,\varrho_2)-1] \times \left( \frac{\rho_1+\rho_2}{\rho_1\rho_2} \sin\left[\frac{\pi}{4}+2z(\varrho_2-\varrho_1)\right] - \frac{1}{\rho_1}\sin\left[\frac{\pi}{4}+2z\varrho_2\right] - \frac{1}{\rho_2}\sin\left[\frac{\pi}{4}-2z\varrho_1\right] \right), \tag{9.19}$$

$$\mathcal{J}_2(z)=\frac{1}{4}\int_{\varrho_2>\varrho_1}\frac{d\varrho_1 d\varrho_2}{(\varrho_1\varrho_2)^{3/2}}(\varrho_2-\varrho_1)^{1/2}[\mathcal{U}_2(\varrho_1,\varrho_2)-1]\times\left(\frac{\rho_1+\rho_2}{\rho_1\rho_2}\cos\left[\frac{\pi}{4}+2z(\varrho_2-\varrho_1)\right]-\frac{1}{\rho_1}\cos\left[\frac{\pi}{4}+2z\varrho_2\right]-\frac{1}{\rho_2}\cos\left[\frac{\pi}{4}-2z\varrho_1\right]\right), \quad (9.20)$$

$$\mathcal{J}_1^+(z)=\frac{1}{4}\int_{\varrho_2>\varrho_1}\frac{d\varrho_1 d\varrho_2}{(\varrho_1\varrho_2)^{3/2}(\varrho_1+\varrho_2)^{1/2}}\left\{[\mathcal{U}_1^+(\varrho_1,\varrho_2)-1]\times\left(\cos\left[\frac{\pi}{4}+2z(\varrho_1+\varrho_2)\right]-\frac{1}{\sqrt{2}}\right)+[\mathcal{U}_2^+(\varrho_1,\varrho_2)-1]\times\left(\sin\left[\frac{\pi}{4}+2z(\varrho_1+\varrho_2)\right]-\frac{1}{\sqrt{2}}\right)\right\}, \quad (9.21)$$

$$\mathcal{J}_2^+(z)=\frac{z}{2}\int_{\varrho_2>\varrho_1}\frac{d\varrho_1 d\varrho_2}{(\varrho_1\varrho_2)^{3/2}}(\varrho_1+\varrho_2)^{1/2}\left\{[\mathcal{U}_1^+(\varrho_1,\varrho_2)-1]\sin\left[\frac{\pi}{4}+2z(\varrho_1+\varrho_2)\right]-[\mathcal{U}_2^+(\varrho_1,\varrho_2)-1]\sin\left[\frac{\pi}{4}-2z(\varrho_1+\varrho_2)\right]\right\}, \quad (9.22)$$

where $z=\omega/\omega_1$ is the dimensionless frequency. The new energy scale is related to the characteristic length $r_{\mathrm{II}}$ in the second regime in the usual way:

$$\omega_1=\frac{v_F}{\sqrt{6}r_{\mathrm{II}}}. \quad (9.23)$$

The second regime corresponds to long distances, $r_{\mathrm{II}}>\xi$, traveled by electron. This is reflected in the fact that the frequency $\omega_1$ is smaller than $\omega_0$, the characteristic frequency for the first regime. Using Eq. (5.29), we can establish the relation between $\omega_0$ and $\omega_1$, namely, $\omega_1\sim\omega_0\varepsilon^{1/6}$, where $\varepsilon$ is the small parameter, defined by Eq. (3.10). We emphasize that the second regime exists only if the condition $\varepsilon\ll 1$ is met.

It is important to compare the scale $\omega_1$ to the "diffusive" energy scale $\omega_{\mathrm{diff}}\sim v_F/l_{\mathrm{tr}}$, where $l_{\mathrm{tr}}$ is the transport mean free path. In regime II, we have[26]

$$l_{\mathrm{tr}}\sim v_F(k_F\xi)^2\left[\frac{v_F h_0^2\xi^3}{\Phi_0^2}\right]^{-1}=\frac{k_F^2\Phi_0^2}{h_0^2\xi}. \quad (9.24)$$

In this estimate, the combination $h_0^2\xi^3 v_F/\Phi_0^2$ stands for a single-particle scattering rate, calculated from the golden rule, with $h_0^2\xi^2/\Phi_0^2$ coming from the square of the matrix element; the factor $(k_F\xi)^2$ accounts for the small-angle scattering. Equation (9.24) leads to the following relation between the transport mean free path and $r_{\mathrm{II}}$:

$$\left(\frac{l_{\mathrm{tr}}}{k_F}\right)^{1/2}\sim r_{\mathrm{II}}\sim\frac{\xi}{\sqrt{\varepsilon}}. \quad (9.25)$$

As follows from Eq. (9.25), the distance $r_{\mathrm{II}}$, over which the phase of the Friedel oscillations is preserved, is intermediate between $l_{\mathrm{tr}}$ and $\xi$. Indeed, the ratio $l_{\mathrm{tr}}/r_{\mathrm{II}}$ is $\sim k_F r_{\mathrm{II}}\sim k_F\xi/\sqrt{\varepsilon}$. This ratio is large both because $k_F\xi\gg 1$ and because $\varepsilon\ll 1$. Thus, we conclude that the energy scale $\omega_1$ is much larger than $\omega_{\mathrm{diff}}$ since $\omega_{\mathrm{diff}}/\omega_1$ is $\sim r_{\mathrm{II}}/l_{\mathrm{tr}}\ll 1$, i.e., the conventional diffusive zero-bias anomaly develops at frequencies much smaller than the width of the zero-bias anomaly in regime II.

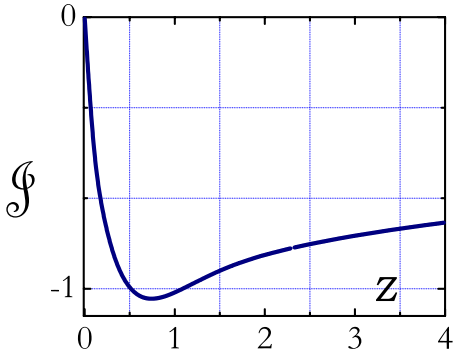


FIG. 15. (Color online) Dimensionless density of states in regime II, $\mathcal{J}(z)=\mathcal{J}^+(z)+\mathcal{J}^-(z)$, is plotted in the units of $(\nu_0\mathcal{D})$ from Eqs. (9.19)–(9.22) versus dimensionless frequency $z=\omega/\omega_1$, where $\omega_1$ is defined by Eq. (9.23) and $\mathcal{D}$ is defined by Eq. (9.18).

### B. Discussion

Dimensionless density of states, $\mathcal{J}=\mathcal{J}^-+\mathcal{J}^+$, is plotted in Fig. 15. It is seen that the function $\mathcal{J}(z)$ exhibits pronounced minimum at $z\approx 0.75$, which is followed by a *monotonous* decay. This behavior should be contrasted to the dimensionless density of states in regime I, plotted in Fig. 14. The difference is that the function $\mathcal{I}$ exhibits damped oscillations with alternating maxima and minima, while $\mathcal{J}$ contains only a single minimum. This difference is not unexpected on qualitative grounds. Indeed, the distance $\sim r_{\mathrm{I}}$, at which the oscillations are formed in regime I, is much smaller than the correlation radius $\xi$, while the characteristic distance $\sim r_{\mathrm{II}}$ in regime II is much bigger than $\xi$. Therefore, it is remarkable that $\mathcal{J}(z)$ exhibits even a single minimum. However, qualitative difference between $\mathcal{I}(z)$ and $\mathcal{J}(z)$ at large $z$ is much harder to trace from their respective representations as double integrals over $\rho_1$ and $\rho_2$ [see Eqs. (8.6) and (9.19)–(9.22)]. The structure of one of several contributions to $\mathcal{I}(z)$ and $\mathcal{J}(z)$ can be loosely rewritten as

$$\int_0^\infty\int_0^\infty\frac{d\rho_1 d\rho_2}{(\rho_1\rho_2)^{3/2}}\sqrt{\rho_1+\rho_2}\frac{\sin z(\rho_1+\rho_2)}{\sqrt{1+\rho_1^2\rho_2^2(\rho_1+\rho_2)^2}}, \quad \text{(I)}, \quad (9.26)$$

$$\int_0^\infty\int_0^\infty\frac{d\rho_1 d\rho_2}{(\rho_1\rho_2)^{3/2}}\sqrt{\rho_1+\rho_2}\frac{\sin z(\rho_1+\rho_2)}{\sqrt{1+\rho_1^2\rho_2^2}}. \quad \text{(II)} \quad (9.27)$$

The integrands in Eqs. (9.26) and (9.27) differ only by the structure of the denominators. This difference can be traced to Eq. (9.8) in which the correlator is set either constant (regime I) or a $\delta$ function (regime II). From the form of the

contribution Eq. (9.26), it is not obvious at all that the large-$z$ behavior is determined by well-defined values $\rho_1=\rho_2=\rho_0$ in the complex plane, with $\rho_0$ satisfying $1+\rho_0^6=0$, so that the contribution is oscillatory Eq. (8.9). This fact was established above by taking the large-$z$ asymptote before the averaging over realizations. It is also supported by numerics in Fig. 14.

Monotonous behavior of $\mathcal{J}(z)$ at large $z$ implies that the integral Eq. (9.27) is not dominated by distinct complex $\rho_1=\rho_2=\tilde{\rho}_0$, such that $1+\tilde{\rho}_0^4=0$. The only vague explanation of this is that the denominator, $\sqrt{1+\rho_1^2\rho_2^2(\rho_1+\rho_2)^2}$, in Eq. (9.26) fixes $\rho_1\approx\rho_2\approx\rho_0$ much more efficiently that the denominator, $\sqrt{1+\rho_1^2\rho_2^2}$, in Eq. (9.27) fixes $\rho_1$, $\rho_2$ near $\tilde{\rho}_0$.

## X. IMPLICATIONS

### A. Half-filled Landau level

The experimental situation of a two-dimensional electron gas placed in an inhomogeneous magnetic field can be created artificially, see, e.g., Refs. 10–18. This situation also emerges in electron gas in a strong constant magnetic field, when the filling factor of the lowest Landau level is close to 1/2. In the latter case, the constant field transforms electrons into composite fermions,[8,9] with well defined Fermi surface,[67–71] while the randomness of the magnetic field is due to spatial inhomogeneity of the electron density. Transport properties of *noninteracting* gas of composite fermions under these conditions were considered theoretically in Refs. 22–30.

With regard to the tunnel density of states near the half-filling, for the case of homogeneous gas, it was addressed theoretically in Refs. 72–74 both for tunneling into the bulk and into the edge. Unlike interacting *homogeneous* electron gas,[4] composite fermions are expected to exhibit a zero-bias anomaly *even without inhomogeneity*.[72–74] This difference between composite fermions and free electrons can be traced to the form of density-density correlator of composite fermions at small momenta.[9] Namely, the pole of this correlator defines the mode of neutral excitations with dispersion $\omega\propto iq^3$, even slower than the diffusive mode in the presence of disorder. The resulting suppression of tunneling into the edge of homogeneous electron gas at half-filling, predicted in Refs. 73 and 74, turned out to be stronger than in the experiment.[75,76]

It is convenient to express the random static magnetic field originating from spatial inhomogeneity with magnitude $\delta n$ in the units of the cyclotron frequency:

$$\frac{\delta\omega_c}{\Omega_{1/2}}=\frac{2\delta n}{n_{1/2}}, \tag{10.1}$$

where $n_{1/2}$ is the concentration of electrons at which the filling factor in the field, $\Omega_{1/2}$, is equal to 1/2. Density fluctuations not only smear out the "intrinsic" zero-bias anomaly but also give rise to the smooth-disorder-induced zero-bias anomaly, studied in this paper. Quantitatively, we predict the following relation between the width of zero-bias anomaly and the magnitude $\delta n$ of the density fluctuations:

$$\omega_0\sim\Omega_{1/2}\left(\frac{\delta n}{n_{1/2}}\right)^{2/3}. \tag{10.2}$$

This relation follows directly from Eq. (3.11) and applies for smooth fluctuations with spatial scale $\xi$ satisfying the condition

$$n_{1/2}\xi^2>\left(\frac{n_{1/2}}{\delta n}\right)^{4/3}. \tag{10.3}$$

This condition is equivalent to the condition $\varepsilon>1$, where the parameter $\varepsilon$ is defined by Eq. (3.10). In the opposite case of "fast" fluctuations, the width $\omega_1$ is given by

$$\omega_1\sim\Omega_{1/2}[n_{1/2}\xi^2]^{1/4}\left(\frac{\delta n}{n_{1/2}}\right), \tag{10.4}$$

as follows from Eq. (3.11). Concerning the magnitude of the anomaly, Eqs. (8.5) and (9.18) predict $\delta\nu/\nu_0\sim(\delta n/n_{1/2})$ for slow fluctuations Eq. (10.2) and $\delta\nu/\nu_0\sim(\delta n/n_{1/2})^{3/2}[n_{1/2}\xi^2]^{3/8}$ for the fast fluctuations Eq. (10.4), respectively.

A qualitative difference between the "intrinsic" zero-bias anomaly[72–74] and inhomogeneity-induced zero-bias anomaly, considered in this paper, is that the latter necessarily involves electron-electron scattering processes with momentum transfer $\approx 2k_F$. As was mentioned above, the intrinsic anomaly gets stronger toward the edge.[73,74] We would like to emphasize that the anomaly due to the $2k_F$ processes also gets stronger toward the edge. The reason is that the average electron concentration decreases monotonically upon approaching the edge. This decrease translates into a *nonfluctuating* magnetic field, acting on composite fermions,[23] which *increases* toward the edge. Correction $\delta\nu(\omega)$ to the density of states in this case is given by Eq. (7.13) and is plotted in Fig. 10. Then, we conclude that the ratio of magnitudes, $\delta\nu_{\text{bulk}}/\delta\nu_{\text{edge}}$, is simply $\sim(\delta n_{\text{bulk}}/\delta n_{\text{edge}})\ll 1$, where $\delta n_{\text{bulk}}$ and $\delta n_{\text{edge}}$ are the deviations of electron density from $n_{1/2}$ in the bulk and at the edge, respectively. The widths of $\delta\nu_{\text{bulk}}(\omega)$ and $\delta\nu_{\text{edge}}(\omega)$ are related as $\sim(\delta n_{\text{edge}}/\delta n_{\text{bulk}})^{2/3}\ll 1$.

### B. Spin-fermion model

Similarly to composite fermions, the dispersion of neutral excitations right at the critical point in the spin-fermion model is dominated by a slow mode,[77,78] $\omega\propto iq^3$. Outside the critical region, the propagator of the neutral excitations (bosons) in the spin-disordered phase has the conventional Ornstein–Zernike form $\chi(q)\propto 1/(q^2+\xi^{-2})$, where $\xi$ is the correlation radius, which diverges at the critical point. Interaction of electrons with slow critical fluctuations can be viewed as scattering by the smooth disorder. The question that we will discuss below is how the growth of $\xi$, upon approaching the critical point, manifests itself in the behavior of the averaged (over the fluctuations of the order parameter) density of states. Our calculations demonstrate that the dimensionless parameter $\varepsilon$, defined by Eq. (3.10), plays a crucial role.

Traditionally, in the studies of the response functions, such as spin susceptibility, of two-dimensional electrons near

the quantum critical point, see, e.g., Refs. 77–82, electrons are treated as ballistic. More specifically, they interact only with critical fluctuations but *not with each other*. Transport at the quantum critical point was also considered for noninteracting ballistic[83] or diffusive[84] electrons that are scattered by bosonic excitations.

In all theoretical treatments of the spin-fermion model, modification of the response of the electron gas due to interaction with bosons was governed by the processes with *small momentum transfer*. Our main point is that incorporating *direct* electron-electron interactions into the spin-fermion model gives rise to a novel feature in the response of the electron gas near the critical point in spin-disordered phase. The underlying reason is that, while critical bosonic fluctuations are "smooth," so that their momenta are $\ll k_F$, electron-electron interactions allow $2k_F$ processes. Then, the physics, discussed in this paper, emerges in the following way:

(i) interaction with slow bosonic fluctuations, curves slightly the electron trajectories;

(ii) interaction between the electrons, moving along slightly curved trajectories, generates a small energy scale, which reflects the "degree" of curving; and

(iii) the degree of curving grows with correlation radius $\xi$ of the bosonic excitations.

As a result, the character of critical fluctuations is reflected in the density of states $\delta\nu(\omega)$ in a very nontrivial fashion. Namely, they give rise to the lively low-frequency feature and even aperiodic oscillations in $\delta\nu(\omega)$, as was demonstrated above. This suggests that information about proximity to the critical point can be inferred from tunneling experiments.

To quantify the above scenario, we will assume for simplicity[85] that bosonic critical fluctuations of magnetization, $\mathbf{S}(\mathbf{r})$, interact with electron spins not as $\boldsymbol{\sigma}\cdot\mathbf{S}$, where $\boldsymbol{\sigma}$ are the Pauli matrices, but via the *position-dependent* Zeeman energy $E_Z(\mathbf{r})$ with characteristic magnitude $E_0$. Assuming that the fluctuations $\mathbf{S}(\mathbf{r})$ are static, we get for correlator of random Zeeman energy $E_Z(\mathbf{r})$ the standard expression

$$\langle E_Z(\mathbf{r})E_Z(\mathbf{r}')\rangle = E_0^2\int\frac{d\mathbf{q}}{2\pi}\frac{e^{i\mathbf{q}(\mathbf{r}-\mathbf{r}')}}{q^2+\xi^{-2}} = E_0^2K_0(|x_1-x_2|/\xi), \tag{10.5}$$

where $K_0$ is the Macdonald function.

As the next step, we notice that the *force* $\nabla E_Z(\mathbf{r})$ curves the electron trajectories *in the same way* as random magnetic field $h(x,y)$. This allows us to use general expressions Eqs. (7.10) and (7.11) for the interaction correction to the density of states. We can also employ the result Eq. (9.8) for the general averaging procedure, i.e., to treat critical fluctuations as a disorder. With the help of Eq. (10.5), the result Eq. (9.8) assumes the form

$$\langle\exp\{2i\delta\varphi_\Sigma^{(-)}\}\rangle = \left[1+iE_0^2\int_0^{r_2}\int_0^{r_2}dx_1dx_2f_-(x_1)f_-(x_2)\partial_{x_1}\partial_{x_2}\times K_0\left(\frac{|x_1-x_2|}{\xi}\right)\right]^{-1/2}, \tag{10.6}$$

where the function $f_-$ is defined by Eq. (9.9) for the case of random magnetic field. For the case of random Zeeman energy, the prefactor $1/\Phi_0k_F^{1/2}$ should be replaced by $k_F^{1/2}/E_F$. Characteristic energy scales can now be inferred from Eq. (10.6) on the basis of the following reasoning. Characteristic distances $r_1$, $r_2$ in Eq. (10.6) are determined by the condition

$$\int_0^{r_2}\int_0^{r_2}dx_1dx_2K_0\left(\frac{|x_1-x_2|}{\xi}\right)\frac{\partial}{\partial x_1}f_-(x_1)\frac{\partial}{\partial x_2}f_-(x_2)\sim\frac{1}{E_0^2}, \tag{10.7}$$

where we performed integration by parts in Eq. (10.6). Then, the characteristic width of a zero-bias anomaly is equal to $\omega\sim v_F/r_1\sim v_F/r_2$.

Recall now that in the case of random magnetic field, double integral in the left-hand side of Eq. (10.7) did not contain derivatives and was $\propto r_2^3$ in regime I and $\propto r_2^2\xi$ in regime II. This is because the function $f_-(x_1)$ is $\sim r_2^{1/2}$ at $x_1\sim r_2$, see Eq. (9.9). Due to the fact that the effective "force" in the spin-fermion model is $\propto\nabla E_Z(\mathbf{r})$, the left-hand side in Eq. (10.7) is $\sim k_Fr_2/E_F^2$ for $\xi\gg r_2$. In this limit, Eq. (10.7) yields (with logarithmic in $\xi/r_2$ accuracy)

$$r_2\sim k_F^{-1}\left(\frac{E_F}{E_0}\right)^2=\xi_c,\quad \omega\sim\frac{E_0^2}{E_F}=E_c. \tag{10.8}$$

Note that $E_c$ is independent of $\xi$. We conclude that, upon approaching the critical point, as the correlation radius exceeds the value $\xi_c$, the zero-bias anomaly "freezes." Its form is shown in Fig. 14, and its magnitude is $\sim(E_0/E_F)^3$. An alternative way to recover the scales Eq. (10.8) is to notice that parameter $\varepsilon$, which is defined by Eq. (3.10) in the context of random magnetic field, in the situation with random Zeeman energy acquires the form $\varepsilon=(k_F\xi)(E_0/E_F)^2$. Then, $\xi_c$ given by Eq. (10.8) corresponds to $\varepsilon=1$, i.e., to the boundary of regime I.

For $\xi<\xi_c$, the integral in the left-hand side of Eq. (10.7) is proportional to $\xi$ and is independent of $r_2$. Then Eq. (10.7) does not have a solution. Therefore, characteristic $r_1$ and $r_2$ in the expression for the density of states are $\sim\xi$, and the width of the anomaly is simply $\sim v_F/\xi=E_c(\xi_c/\xi)$. Concerning the magnitude of the anomaly at $\xi<\xi_c$, it should be estimated with the account that the integral in the right-hand side of Eq. (10.6) is smaller than 1 *for all* $r_2$. Therefore, $\langle\exp\{2i\delta\varphi_\Sigma^{(-)}\}\rangle$ in Eq. (10.6) can be approximately replaced by $\{1-(i/2\xi_c)[r_2\Theta(\xi-r_2)+\xi\Theta(r_2-\xi)]\}$, where the second term is a small correction. However, only this correction causes a zero-bias anomaly. By substituting this correction into Eq. (7.11), we find the estimate for the magnitude,

$$\frac{\delta\nu}{\nu_0}\sim\left(\frac{E_0}{E_F}\right)^3\left(\frac{\xi_c}{\xi}\right)^{1/2}\sim\left(\frac{E_0}{E_F}\right)^2\frac{1}{(k_F\xi)^{1/2}}. \tag{10.9}$$

We conclude that, as $\xi$ grows and approaches $\xi_c$, the magnitude of the anomaly falls off as $1/\sqrt{\xi}$, and the anomaly narrows as $1/\xi$.

The remaining issue to discuss is whether or not the assumption that fluctuating Zeeman energy $E_Z(\mathbf{r})$ is static applies at relevant frequency and spatial scales, $E_c$ and $\xi_c$. For this purpose, we recall that the correlator of Zeeman energies in the momentum space does not have a simple Ornstein–

Zernike form but is rather $\langle|E_Z(\mathbf{q})|^2\rangle \propto 1/(q^2+\xi^{-2}+\varsigma\omega/q)$, where the dynamic term $\varsigma\omega/q$ describes the damping of bosons due to creation of electron-hole pairs. The prefactor $\varsigma$ (the Landau damping coefficient) is thus quadratic in coupling of electrons to the spin density fluctuations, i.e., $\varsigma \propto E_0^2$. For characteristic frequencies, the dynamic term $\varsigma(\omega/q) \sim \varsigma E_c \xi_c \sim \varsigma v_F$. Therefore, it is negligible only if the condition $\xi_c^{-2}=k_F^2(E_0/E_F)^4 \gg \varsigma v_F$ holds. With $\varsigma$ being proportional to $E_0^2$, the above condition is met for large enough coupling, $E_0$. In the opposite case, when the dynamic part of correlator dominates at $\omega \sim E_c$ and $q \sim \xi_c^{-1}$, the zero-bias anomaly develops only away from the critical point when $\xi$ becomes smaller than $(\varsigma v_F)^{-1/2}$. Upon further departure from the critical point, our prediction $\delta\nu/\nu_0 \propto \xi^{-1/2}$ and $\omega \sim v_F/\xi$ should apply. Note finally that *directly at the critical point*, the slow mode $\omega \approx iq^3/\varsigma$ gives rise to the intrinsic zero-bias anomaly,[81] similar to the composite fermions.

## ACKNOWLEDGMENTS

The authors acknowledge the support of NSF (Grant No. DMR-0503172) and of the Petroleum Research Fund (Grant No. 43966-AC10). The authors are grateful to E. G. Mishchenko and O. A. Starykh for numerous discussions.

## APPENDIX A: POLARIZATION OPERATOR IN THE COORDINATE SPACE

Here, we derive Eqs. (4.2) and (4.3) for polarization operator in coordinate space using the known expression[59] for $\Pi(\mathbf{q},\omega)$ in the momentum space. Since we are interested in the behavior of $\Pi(\mathbf{r},\omega)$ at distances $|\mathbf{r}| \gg k_F^{-1}$, it is sufficient to perform the Fourier transform

$$\Pi(\mathbf{r},\omega) = \frac{1}{2\pi}\int d\mathbf{q} e^{i\mathbf{q}r}\Pi(\mathbf{q},\omega) \tag{A1}$$

using the asymptotes of $\Pi(\mathbf{q},\omega)$ at small $q \ll k_F$ and at $q$ close to $2k_F$. The small-$q$ asymptote of $\Pi(\mathbf{q},\omega)$ has the form

$$\Pi_0(\mathbf{q},\omega) = -\nu_0\left[1 + \frac{i\omega\Theta(qv_F-\omega)}{\sqrt{q^2v_F^2-\omega^2}} + \frac{\omega\Theta(\omega-qv_F)}{\sqrt{\omega^2-q^2v_F^2}}\right], \tag{A2}$$

where $\Theta(x)$ is the step function. The easiest way to perform the integration Eq. (A1) is to first Fourier transform Eq. (A2) with respect to *frequency*:

$$-\frac{\Theta(qv_F-\omega)}{\sqrt{q^2-(\omega/v_F)^2}} + \frac{i\Theta(\omega-qv_F)}{\sqrt{(\omega/v_F)^2-q^2}} = \int_0^\infty ds J_0(qs)\exp\left\{\frac{i\omega s}{v_F}\right\}. \tag{A3}$$

Substituting Eq. (A2) into Eq. (A3) and using the orthogonality relation $\int_0^\infty dqqJ_0(qs)J_0(qr)=\delta(r-s)/r$, we readily obtain

$$\Pi_0(\mathbf{r},\omega) = -\frac{i\nu_0\omega}{v_F r}\exp\left\{\frac{i\omega r}{v_F}\right\}. \tag{A4}$$

In order to calculate $\Pi_{2k_F}(\mathbf{r},\omega)$, we use the form of the polarization operator in momentum space for $|q-2k_F| \ll k_F$ and $\omega \ll E_F$:

$$\Pi_{2k_F}(\mathbf{q},\omega) = \nu_0\left[1 - \frac{1}{\sqrt{4k_F}}(\sqrt{q-2k_F+\omega/v_F} + \sqrt{q-2k_F-\omega/v_F})\right], \tag{A5}$$

where the square roots should be understood as $\sqrt{x} \to \mathrm{sign}(x)\sqrt{x}$. Then, the integral over $\mathbf{q}$ in Eq. (A1) assumes the form

$$\begin{aligned}\Pi_{2k_F}(\mathbf{r},\omega) &= -\nu_0\int_0^\infty dqqJ_0(qr)[\sqrt{q-2k_F+\omega/v_F} + \sqrt{q-2k_F-\omega/v_F}] \\ &\times \approx \sqrt{\frac{4k_F}{\pi r}}\int_0^\infty dq\cos\left(qr-\frac{\pi}{4}\right) \\ &\times[\sqrt{q-2k_F+\omega/v_F}+\sqrt{q-2k_F-\omega/v_F}],\end{aligned} \tag{A6}$$

where we used the fact that $k_F r \gg 1$ and replaced the Bessel function by its large-$q$ asymptotics. Integration over variable $q$ in Eq. (A6) is performed with the use of the identity

$$\int_a^\infty dz\cos z\sqrt{z-a} = \frac{\sqrt{\pi}}{2}\sin\left(a+\frac{\pi}{4}\right) \tag{A7}$$

and yields the zero-temperature limit of Eq. (4.3).

## APPENDIX B: POLARIZATION OPERATOR IN A CONSTANT MAGNETIC FIELD

We start from the general expression[63] for the polarizability in arbitrary magnetic field:

$$\begin{aligned}\Pi(q) = -\frac{2m}{\pi}\sum_{n_1=0}^\infty\sum_{n_2=0}^\infty \frac{(-1)^{(n_2-n_1)}(f_{n_1}-f_{n_2})}{n_2-n_1} \\ \times\exp(-q^2l^2/2)L_{n_1}^{n_2-n_1}\left(\frac{q^2l^2}{2}\right)L_{n_2}^{n_1-n_2}\left(\frac{q^2l^2}{2}\right),\end{aligned} \tag{B1}$$

where $L_{n_1}^{n_2-n_1}(x)$ and $L_{n_2}^{n_1-n_2}(x)$ are the Laguerre polynomials, and $f_n=\{\exp[(n-N_F)\hbar\omega_c/T]+1\}^{-1}$ is the Fermi distribution. At small $q \ll k_F$, Eq. (B1) yields[63] $\Pi(q)=-(m/\pi)[1-J_0^2(qR_L)]$, i.e., the characteristic scale is $q \sim R_L^{-1}$. For $(q-2k_F) \ll k_F$, it is convenient to perform the summation over the Landau levels with the help of the following integral representation of the Laguerre polynomial:

$$L_m^n(x) = \frac{1}{2\pi}\int_0^{2\pi}\frac{d\theta}{(1-e^{i\theta})^{n+1}}\exp\left\{\frac{xe^{i\theta}}{e^{i\theta}-1} - im\theta\right\}. \tag{B2}$$

In the vicinity $q=2k_F$, Eq. (B2) contains a small factor $\exp(-q^2l^2/2)$. This factor is compensated by the product of Laguerre polynomials since each of them is $\propto\exp(x/2)$, which comes from the exponent in Eq. (B2) taken at $\theta=\pi$. With contribution from the vicinity $\theta=\pi$ dominating the integral (B2), we can expand the integrand around this point as

$\exp[x/2+i\pi m+i\phi(\psi)]/2^{n+1}$, where $\psi=(\theta-\pi)$, and the phase $\phi(\psi)$ is equal to

$$\phi(\psi)=\left(\frac{x}{4}-m-\frac{n+1}{2}\right)\psi+\frac{x\psi^3}{48}. \tag{B3}$$

Now, we make use of the fact that only a relatively small number $\sim(k_F l)^{2/3}\ll N_F$ of Landau levels around $E_F$ contribute to the sum Eq. (B2). This suggests that we can present $n_1$ and $n_2$ as $n_1=N_F+m_1$ and $n_2=N_F-m_2$, respectively, and extend the sum over $m_1$, $m_2$ from $-\infty$ to $+\infty$. After that, the summation over Landau levels can be easily carried out with the help of the following identity:

$$\sum_{m_1,m_2=-\infty}^{\infty}\frac{f_{N_F-m_1}-f_{N_F+m_2}}{m_1+m_2}\cos[(m_1-m_2)\alpha+\beta]$$
$$=\frac{2\pi^2 T\cos\beta}{\hbar\omega_c\sinh(2\pi|\alpha|T/\hbar\omega_c)}. \tag{B4}$$

As the next step, we substitute the representation Eq. (B2) of Laguerre polynomials with the integrand expanded according to Eq. (B3) into Eq. (B1). Upon this substitution, we perform the summation over Landau levels using the relation Eq. (B4). Then, the double integral, which emerges in Eq. (B1) as a result of representing the two Laguerre polynomials Eq. (B2), assumes the form

$$\int_{-\infty}^{\infty}\int_{-\infty}^{\infty}\frac{d\psi_1 d\psi_2}{|\psi_1+\psi_2|}\cos\left[(\psi_1^3+\psi_2^3)\frac{N_F}{12}-(\psi_1+\psi_2)\frac{\delta q R_L}{2}\right], \tag{B5}$$

where $\delta q=q-2k_F$. Note that integration over the difference $(\psi_1-\psi_2)$ in Eq. (B5) can be performed explicitly. It is convenient to present the final result not for $\Pi(q)$ but rather for the derivative $\Pi'(q,T)=\partial\Pi(q,T)/\partial q$. Knowledge of $\Pi'(q,T)$ is sufficient for finding the large-distance behavior of the potential, created by the short-range impurity. Indeed, this potential can be expressed directly through $\Pi'(2k_F+Q)$ as follows:

$$V_H(r)=\frac{V(2k_F)g}{2(\pi k_F r)^{3/2}}\int_{-\infty}^{\infty}dQ\sin\left[(2k_F+Q)r-\frac{\pi}{4}\right]$$
$$\times\Pi'(2k_F+Q,T). \tag{B6}$$

At zero temperature and in a zero magnetic field, we have $\Pi'(q,0)\propto\theta(\delta q)/\sqrt{\delta q}$. At finite magnetic field and finite temperature, taking the derivative of Eq. (B5) with respect to $\delta q$, we arrive at the result

$$\Pi'(q,T)=-\frac{2^{1/3}mT}{(\pi k_F p_0)^{1/2}\epsilon_0}\int_0^{\infty}\frac{dx x^{1/2}}{\sinh(2\pi xT/\epsilon_0)}$$
$$\times\sin\left(2^{2/3}\frac{\delta q}{p_0}x+\frac{1}{3}x^3+\frac{\pi}{4}\right). \tag{B7}$$

In the limit $T\to 0$, substitution of Eq. (B7) into Eq. (B6) and integration over $Q$ reproduces Eq. (3.1).

Interestingly, for $T=0$, the integral Eq. (B7) can be evaluated analytically:

$$\Pi'(q)=-\frac{m}{(k_F p_0)^{1/2}}\mathrm{Ai}\left(\frac{\delta q}{p_0}\right)\mathrm{Bi}\left(\frac{\delta q}{p_0}\right), \tag{B8}$$

where $\mathrm{Ai}(z)$ is the Airy function and $\mathrm{Bi}(z)$ is another solution of the Airy equation defined, e.g., in Ref. 86. It is seen that the singularity at $q=2k_F$ is smeared by the magnetic field in a rather peculiar way: for positive $\delta q\gg p_0$, the $(\delta q)^{-1/2}$ zero-field behavior [see Eq. (A6)] is restored. However, for large negative $\delta q/p_0$, the derivative $\Pi'(q)$ approaches zero *with oscillations*, namely, as $\cos[4(|\delta q|/p_0)^{3/2}/3]/(|\delta q|)^{1/2}$. As the difference $2k_F-q$ increases and becomes comparable to $k_F$, these oscillations cross over to the "classical" oscillations[63] $\Pi'(q)\propto J_0(qR_L)J_1(qR_L)\propto\cos(2qR_L)$.

## APPENDIX C: EVALUATION OF THE FUNCTIONAL INTEGRAL

Upon combining Eqs. (5.24) and (5.26), the quadratic form in the exponent in the numerator of the functional integral Eq. (5.18) assumes the form

$$2i\delta\varphi(r)-W\{h\}=\frac{2i\varepsilon r^3}{\xi^3}\left\{\frac{1}{12}\left[\int dq\mathcal{A}_{0,q}\right]^2+\sum_{n>0}c_n\left|\int dq\mathcal{A}_{n,q}\right|^2+\int dq\mathcal{A}_{0,q}\mathcal{G}\{\mathcal{A}_n\}\right\}$$
$$-\frac{2r}{\gamma\xi}\sum_{n>0}\int dq\frac{|\mathcal{A}_{n,q}|^2}{\tilde{\mathcal{K}}(q)}-\frac{r}{\gamma\xi}\int dq\frac{|\mathcal{A}_{0,q}|^2}{\tilde{\mathcal{K}}(q)}, \tag{C1}$$

with numerical coefficients $c_n=1/2\pi^2n^2$ and $b_n=-c_n+i/2\pi n$ defined by Eq. (5.27). In the above expression, we had introduced the shorthand notation

$$\mathcal{G}\{\mathcal{A}_{n,q}\}=\sum_{n>0}\left[b_n\int dq\mathcal{A}_{n,q}+b_n^*\int dq\mathcal{A}_{n,q}^*\right]. \tag{C2}$$

We adopt the following sequence of integration over the variables $\mathcal{A}_{n,q}$. First, we integrate over $\mathcal{A}_{0,q}$ using the following decoupling:

$$H\{\mathcal{G}\}=\int\prod_q d\mathcal{A}_{0,q}\exp\left\{-\frac{r}{\gamma\xi}\int dq\frac{|\mathcal{A}_{0,q}|^2}{\tilde{\mathcal{K}}(q)}+\frac{i\varepsilon r^3}{6\xi^3}\left[\int dq\mathcal{A}_{0,q}\right]^2+i\mathcal{G}\int dq\mathcal{A}_{0,q}\right\}$$
$$=e^{-i\pi/4}\sqrt{\frac{3r^3}{2\pi\varepsilon\xi^3}}\int\prod_q d\mathcal{A}_{0,q}d\mathcal{B}_0\exp\left\{-\frac{3ir^3\mathcal{B}_0^2}{2\varepsilon\xi^3}+i\mathcal{B}_0\int dq\mathcal{A}_{0,q}-\frac{r}{\gamma\xi}\int dq\frac{|\mathcal{A}_{0,q}|^2}{\tilde{\mathcal{K}}(q)}+i\mathcal{G}\int dq\mathcal{A}_{0,q}\right\}, \tag{C3}$$

where we had introduced an auxiliary variable $\mathcal{B}_0$. The function $H\{\mathcal{G}\}$ combines all integrals in Eq. (C1) containing $\mathcal{A}_{0,q}$. Subsequent integration first over the variables $\mathcal{A}_{0,q}$ and then over the auxiliary variable $\mathcal{B}_0$ yields

$$H\{\mathcal{G}\} = \sqrt{\frac{\pi\xi\gamma}{ir\int dq\tilde{\mathcal{K}}(q)}}\frac{\exp\{i\mathcal{F}(r)\mathcal{G}^2\}}{\sqrt{1-\frac{2i}{3}\left(\frac{r}{r_{II}}\right)^2}},$$

where we had used the definition $r_{II}=2\xi/(\sqrt{2\pi}\gamma\varepsilon)^{1/2}$. In Eq. (C4), the complex function $\mathcal{F}(r)$ is defined as

$$\mathcal{F}(r) = -\frac{3\varepsilon^{1/2}\left[\gamma\int dq\tilde{\mathcal{K}}(q)\right]^{3/2}}{16\left(\frac{r}{r_{II}}\right)^3+24i\left(\frac{r}{r_{II}}\right)}. \tag{C4}$$

As a result of integration over $\mathcal{A}_{0,q}$ the exponent in the functional integral Eq. (C1) assumes the form

$$i\sum_{n>0}\tilde{c}_n\left|\int dq\mathcal{A}_{n,q}\right|^2-\frac{2r}{\gamma\xi}\sum_{n>0}\int dq\frac{|\mathcal{A}_{n,q}|^2}{\tilde{\mathcal{K}}(q)}+i\mathcal{F}(r)\mathcal{G}^2, \tag{C5}$$

where $\tilde{c}_n$ is related to $c_n$ via a dimensionless factor:

$$\tilde{c}_n = \frac{2\varepsilon r^3}{\xi^3}c_n. \tag{C6}$$

The first and third terms in Eq. (C5) contain squares of the linear combinations of $\mathcal{A}_{n,q}$. To decouple these squares, we introduce a set of auxiliary variables $\alpha_n, \alpha_n^*$ for the first term and one auxiliary variable $\alpha_0$ for the third term as follows:

$$e^{i\mathcal{V}\left|\int dq\mathcal{A}_{n,q}\right|^2} = \frac{1}{2\pi}\int d\alpha_n d\alpha_n^*\exp\left\{-i|\alpha_n|^2+\mathcal{V}^{1/2}\alpha_n^*\int dq\mathcal{A}_{n,q}-\mathcal{V}^{1/2}\alpha_n\int dq\mathcal{A}_{n,q}^*\right\}, \tag{C7}$$

$$e^{i\mathcal{F}(r)\mathcal{G}^2} = \frac{1}{\sqrt{4\pi\mathcal{F}(r)}}\int_{-\infty}^{\infty}d\alpha_0\exp\left\{-\frac{i\alpha_0^2}{4\mathcal{F}(r)}+i\alpha_0\mathcal{G}\right\}. \tag{C8}$$

Note that $\mathrm{Im}[1/\mathcal{F}(r)]<0$, so that the decoupling Eq. (C8) of the quadratic in $\mathcal{G}$ term in the exponent of Eq. (C4) is justified.

As the next step, we perform Gaussian integration over the infinite set of variables $\{\mathcal{A}_{n,q}\}$:

$$\int d\mathcal{A}_{n,q}d\mathcal{A}_{n,q}^*\exp\left\{\int dq\left[-\frac{2r|\mathcal{A}_{n,q}|^2}{\gamma\xi\tilde{\mathcal{K}}(q)}+\mathcal{A}_{n,q}(\tilde{c}_n^{1/2}\alpha_n^*+i\alpha_0 b_n)+\mathcal{A}_{n,q}^*(-\tilde{c}_n^{1/2}\alpha_n+i\alpha_0 b_n^*)\right]\right\}$$
$$=\frac{2i\pi}{(2r/\gamma\xi)\int dq[\tilde{\mathcal{K}}(q)]^{-1}}\exp\left\{-|-i\tilde{c}_n^{1/2}\alpha_n^*+\alpha_0 b_n|^2\frac{\gamma\xi}{2r}\int dq\tilde{\mathcal{K}}(q)\right\}. \tag{C9}$$

As follows from Eqs. (C7) and (C9), the integrals over all $\alpha_n$ are Gaussian and can be easily evaluated:

$$\int\frac{d\alpha_n d\alpha_n^*}{2\pi}\exp\left\{-i|\alpha_n|^2-|-i\tilde{c}_n^{1/2}\alpha_n^*+\alpha_0 b_n|^2\frac{\gamma\xi}{2r}\int dq\tilde{\mathcal{K}}(q)\right\}$$
$$=\frac{2r}{2r-i\gamma\xi\tilde{c}_n\int dq\tilde{\mathcal{K}}(q)}\exp\left\{-\frac{\gamma\xi\alpha_0|b_n|^2}{2r}\int dq\tilde{\mathcal{K}}(q)-\frac{\tilde{c}_n\left[\alpha_0|b_n|\gamma\xi\int dq\tilde{\mathcal{K}}(q)\right]^2}{4ir^2+2r\gamma\xi\tilde{c}_n\int dq\tilde{\mathcal{K}}(q)}\right\}. \tag{C10}$$

The remaining integral over $\alpha_0$ is also Gaussian. Note now that the denominator in Eq. (5.18), responsible for the normalization, can be evaluated by performing the same steps as above. This evaluation amounts to setting $\tilde{c}_n=0$ in Eq. (C10) and taking the limit $r_{II}\to\infty$ in Eq. (C4). As a result, the functional integral reduces to the ratio of the ordinary integrals:

$$\langle e^{2i\delta\varphi(r)}\rangle = \frac{1}{\sqrt{1-\frac{2i}{3}\left(\frac{r}{r_{II}}\right)^2}}\left[\prod_{n=1}^{\infty}\frac{n^2}{n^2-2i(r/r_{II})^2/\pi^2}\right]\times\frac{\int_{-\infty}^{\infty}d\alpha_0\exp\{-w\alpha_0-u_1\alpha_0^2\}}{\int_{-\infty}^{\infty}d\alpha_0\exp\{-w\alpha_0-u_0\alpha_0^2\}}, \tag{C11}$$

where the coefficients $w$ and $u_0$ are defined as

$$w=\frac{\gamma\xi}{2r}\left[\sum_{n>0}|b_n|^2\right]\int dq\tilde{\mathcal{K}}(q),$$
$$u_0=\frac{r}{\xi}\left(\int dq\tilde{\mathcal{K}}(q)\right)^{-3/2}, \tag{C12}$$

while the definition of the coefficient $u_1$ is the following:

$$u_1=\frac{i}{4\mathcal{F}(r)}+\left[\gamma\xi\int dq\tilde{\mathcal{K}}(q)\right]^2\sum_{n>1}\frac{\tilde{c}_n|b_n|^2}{4ir^2+2r\gamma\xi\tilde{c}_n\int dq\tilde{\mathcal{K}}(q)}. \tag{C13}$$

For characteristic $r\sim r_{II}$, the first term in Eq. (C13) is $\sim\varepsilon^{-1/2}$, as follows from Eq. (C4). On the other hand, the product $r\xi\tilde{c}_n$ in the denominator of the second term in Eq. (C13) is $\sim\varepsilon r^4/\xi^2\sim r^4/r_{II}^2$. Thus, for $r\sim r_{II}$, both terms in the denominator of the sum in the second term are $\sim r_{II}^2$. The numerator in the sum over $n$ is $\sim\varepsilon^{-1/2}$ for $r\sim r_{II}$. Then, the estimate for the second term in Eq. (C13) is $\xi^2/r_{II}^2\varepsilon^{1/2}$, so that the second term is smaller than the first term in parameter $\xi^2/r_{II}^2\sim\varepsilon$. Next, we notice that for $r\sim r_{II}$, both $u_0$ and $u_1$ are of the same order and are $\sim\varepsilon^{-1/2}$. On the other hand, as seen from

Eq. (C12), the parameter $w$ for $r \sim r_{II}$ is small, $w \sim \varepsilon^{1/2}$. This allows us to disregard $w$ both in the numerator and denominator in Eq. (C11), so that the ratio of integrals reduces to $(u_0/u_1)^{1/2}$. Using Eq. (C4), this ratio can be rewritten as $[1-(2i/3)(r/r_{II})^2]^{-1/2}$. Substituting it into Eq. (C11), we arrive at Eq. (5.28) in Sec. V.

## APPENDIX D: ANALYSIS OF THE INTEGRALS EQUATION (8.6)

The dimensionless function $\mathcal{I}(z)$ defined by Eq. (8.6) can be naturally divided into two parts, $\mathcal{I}(z)=\mathcal{I}_+ + \mathcal{I}_-$, where

$$\mathcal{I}_-(z) = \int_{\rho_2>\rho_1} \frac{d\rho_2 d\rho_1}{(\rho_2\rho_1)^{3/2}} \int_0^z dz' \sin[(z-z')(\rho_2+\rho_1)] \times \sqrt{\rho_2-\rho_1} \Bigg\{ \sin[\pi/4+(z+z')(\rho_2-\rho_1)] \times \sqrt{\frac{1+\sqrt{1+\rho_2^2\rho_1^2(\rho_2-\rho_1)^2}}{1+\rho_2^2\rho_1^2(\rho_2-\rho_1)^2}} + \cos[\pi/4+(z+z')(\rho_2-\rho_1)] \sqrt{\frac{\sqrt{1+\rho_2^2\rho_1^2(\rho_2-\rho_1)^2}-1}{1+\rho_2^2\rho_1^2(\rho_2-\rho_1)^2}} \Bigg\} \tag{D1}$$

and

$$\mathcal{I}_+(z) = \int_{\rho_2>\rho_1} \frac{d\rho_2 d\rho_1}{(\rho_2\rho_1)^{3/2}} \int_0^z dz' \sin[(z-z')(\rho_2+\rho_1)] \times \sqrt{\rho_2+\rho_1} \Bigg\{ \sin[\pi/4-(z+z')(\rho_2+\rho_1)] \times \sqrt{\frac{1+\sqrt{1+\rho_2^2\rho_1^2(\rho_2+\rho_1)^2}}{1+\rho_2^2\rho_1^2(\rho_2+\rho_1)^2}} + \cos[\pi/4-(z+z')(\rho_2+\rho_1)] \sqrt{\frac{\sqrt{1+\rho_2^2\rho_1^2(\rho_2+\rho_1)^2}-1}{1+\rho_2^2\rho_1^2(\rho_2+\rho_1)^2}} \Bigg\}. \tag{D2}$$

The complexity in numerical evaluation of $\mathcal{I}_+$ and $\mathcal{I}_-$ stems from the fact that, upon integration over $z'$, both integrals turn into the sums of two contributions, each of which is *divergent* in the limit $z \to 0$. Therefore, it is necessary to rewrite the result of integration over $z'$ in $\mathcal{I}_+$ and in $\mathcal{I}_-$ in such a way that cancellation of the divergent contributions is explicit.

We start with $\mathcal{I}_-$. Integration over $z'$ generates the combination of three terms:

$$\frac{\rho_1+\rho_2}{\rho_1\rho_2}\cos\left[\frac{\pi}{4}+2z(\rho_1-\rho_2)\right] - \frac{1}{\rho_2}\cos\left(\frac{\pi}{4}+2z\rho_1\right) - \frac{1}{\rho_1}\cos\left(\frac{\pi}{4}-2z\rho_2\right). \tag{D3}$$

In order to treat all these three terms on an equal footing, in the first term of Eq. (D3), we introduce the following new variables:

$$\tilde{z} = z(\rho_2-\rho_1),$$

$$x = \frac{\rho_2\rho_1}{z^3(\rho_2-\rho_1)^2}. \tag{D4}$$

In the second term, we introduce $\tilde{z}=z\rho_1$, and finally, in the third term, $\tilde{z}=z\rho_2$. After that, the expression for $\mathcal{I}_-$ assumes the form

$$\mathcal{I}_-(z) = \frac{1}{\sqrt{2}z^3}\int_0^\infty \frac{dx}{x^{5/2}}[F_1(x)-F_1(0)] + \frac{1}{\sqrt{2}z^3}\int_0^\infty \frac{dx}{x^{5/2}}F_2(x,z) + \frac{1}{\sqrt{2}z^3}\int_0^{1/4z^3} \frac{dx}{x^{5/2}}[F_3(x,z)-F_3(0,0)], \tag{D5}$$

where the functions $F_1$, $F_2$, and $F_3$ are defined as

$$F_1(x) = \int_0^\infty \frac{d\tilde{z}}{\tilde{z}^{5/2}} \Bigg\{ (\cos 2\tilde{z}-\sin 2\tilde{z}) \sqrt{\frac{\sqrt{1+\tilde{z}^6x^2}-1}{1+\tilde{z}^6x^2}} + (\cos 2\tilde{z}+\sin 2\tilde{z}) \sqrt{\frac{1+\sqrt{1+\tilde{z}^6x^2}}{1+\tilde{z}^6x^2}} \Bigg\}, \tag{D6}$$

$$F_2(x,z) = \frac{\sqrt{\frac{1}{4}+xz^3}-\frac{1}{2}}{2\sqrt{\frac{1}{4}+xz^3}} \int_0^\infty \frac{d\tilde{z}}{\tilde{z}^{5/2}} \Bigg\{ (\sin 2\tilde{z}-\cos 2\tilde{z}) \times \sqrt{\frac{\sqrt{1+\tilde{z}^6x^2}+1}{1+\tilde{z}^6x^2}} - (\cos 2\tilde{z} + \sin 2\tilde{z}) \sqrt{\frac{\sqrt{1+\tilde{z}^6x^2}-1}{1+\tilde{z}^6x^2}} \Bigg\}, \tag{D7}$$

$$F_3(x,z) = -\frac{\left(\sqrt{\frac{1}{4}-xz^3}+\frac{1}{2}\right)^3 + \left(\sqrt{\frac{1}{4}-xz^3}-\frac{1}{2}\right)^3}{2\sqrt{\frac{1}{4}-xz^3}} \times \int_0^\infty \frac{d\tilde{z}}{\tilde{z}^{5/2}} \Bigg\{ (\cos 2\tilde{z}+\sin 2\tilde{z}) \sqrt{\frac{\sqrt{1+\tilde{z}^6x^2}+1}{1+\tilde{z}^6x^2}} + (\cos 2\tilde{z}-\sin 2\tilde{z}) \sqrt{\frac{\sqrt{1+\tilde{z}^6x^2}-1}{1+\tilde{z}^6x^2}} \Bigg\}. \tag{D8}$$

Subtraction of $x=0$ values from $F_1(x)$ and $F_3(x,z)$ in Eq. (D5) ensures the convergence of integrals over $\tilde{z}$ in Eqs. (D6) and (D8). On the other hand, this subtraction shifts $\mathcal{I}_-$ by $z$-independent constant.

It is seen that in the limit $z \to 0$, the difference $F_2(x,z) - F_2(0,z)$ behaves as $z^3$, so that the contribution from $F_2$ to $\mathcal{I}_-(z)$ remains finite in this limit. On the other hand, the contributions from $F_1$ and $F_3$ both behave as $1/z^3$. To demonstrate that the two divergent contributions cancel out, we divide the integration domain in the first term of $\mathcal{I}_-$ into the intervals $\{0, 1/4z^3\}$ and $\{1/4z^3, \infty\}$. We then combine the two integrals from 0 to $1/4z^3$ to obtain

$$\mathcal{I}_-(z)=\frac{1}{\sqrt{2}z^3}\int_0^{1/4z^3}\frac{dx}{x^{5/2}}\{[F_1(x)-F_1(0)]+[F_3(x,z)-F_3(0,z)]\}+\frac{1}{\sqrt{2}z^3}\int_{1/4z^3}^{\infty}\frac{dx}{x^{5/2}}[F_1(x)-F_1(0)]+\frac{1}{\sqrt{2}z^3}\int_0^{\infty}\frac{dx}{x^{5/2}}F_2(x,z). \tag{D9}$$

The second and third terms in Eq. (D9) are convergent in the limit $z\to 0$. The integrand in the first term has the form

$$F_1(x)-F_1(0)+F_3(x,z)-F_3(0,z)=\left\{1-\frac{\left(\sqrt{\frac{1}{4}-xz^3}+\frac{1}{2}\right)^3+\left(\sqrt{\frac{1}{4}-xz^3}-\frac{1}{2}\right)^3}{2\sqrt{\frac{1}{4}-xz^3}}\right\}\times\int_0^{\infty}\frac{d\tilde{z}}{\tilde{z}^{5/2}}\left\{(\cos 2\tilde{z}+\sin 2\tilde{z})\left[\sqrt{\frac{\sqrt{1+\tilde{z}^6x^2}+1}{1+\tilde{z}^6x^2}}-\sqrt{2}\right]+(\cos 2\tilde{z}-\sin 2\tilde{z})\sqrt{\frac{\sqrt{1+\tilde{z}^6x^2}-1}{1+\tilde{z}^6x^2}}\right\}. \tag{D10}$$

We see that in the limit $z\to 0$, the expression in the curly brackets behaves as $\propto z^3$, and thus cancels the divergent prefactor. Now all three terms in Eq. (D9) yield a finite contribution at $z\to 0$. Our numerical results for $\mathcal{I}_-(z)$ were obtained from Eq. (D9).

We now turn to $\mathcal{I}_+(z)$. In order to deal with small-$z$ behavior in the integral Eq. (D2), we introduce, after performing integration over $z'$, the following new variables:

$$\tilde{z}=z(\rho_2+\rho_1),\qquad x=\frac{\rho_2\rho_1}{z^3(\rho_2+\rho_1)^2}. \tag{D11}$$

Then one obtains $\mathcal{I}_+=\mathcal{I}_+^1+\mathcal{I}_+^2$, where the two contributions are given by

$$\mathcal{I}_+^{(1)}=\frac{1}{\sqrt{2}}\int_0^{1/4z^3}\frac{dx}{x^{3/2}\sqrt{\frac{1}{4}-xz^3}}\int_0^{\infty}\frac{d\tilde{z}}{\tilde{z}^{5/2}}\left\{(1-\sin 2\tilde{z}-\cos 2\tilde{z})\sqrt{\frac{\sqrt{1+\tilde{z}^6x^2}-1}{1+\tilde{z}^6x^2}}-(1-\cos 2\tilde{z}+\sin 2\tilde{z})\left[\sqrt{\frac{\sqrt{1+\tilde{z}^6x^2}+1}{1+\tilde{z}^6x^2}}-\sqrt{2}\right]\right\} \tag{D12}$$

and

$$\mathcal{I}_+^{(2)}=\frac{2}{\sqrt{2}}\int_0^{1/4z^3}\frac{dx}{x^{3/2}\sqrt{\frac{1}{4}-xz^3}}\int_0^{\infty}\frac{d\tilde{z}}{\tilde{z}^{3/2}}\times\left\{(\sin 2\tilde{z}-\cos 2\tilde{z})\sqrt{\frac{\sqrt{1+\tilde{z}^6x^2}-1}{1+\tilde{z}^6x^2}}+(\cos 2\tilde{z}+\sin 2\tilde{z})\left[\sqrt{\frac{\sqrt{1+\tilde{z}^6x^2}+1}{1+\tilde{z}^6x^2}}-\sqrt{2}\right]\right\}. \tag{D13}$$

Both these contributions are finite in the limit $z\to 0$.

## APPENDIX E: ANALYSIS OF THE INTEGRALS EQUATIONS (7.23) and (7.24)

In the integral Eq. (7.23), we perform the following change of variables:

$$\rho_1=\frac{z}{2}\left(1-\sqrt{\frac{v}{v+4}}\right),\qquad \rho_2=\frac{z}{2}\left(1+\sqrt{\frac{v}{v+4}}\right), \tag{E1}$$

after which it acquires the form

$$P_1^+(x)=\frac{3(2^{13/6})}{\pi^{3/2}}\int_0^{\infty}\frac{dv}{v^{1/2}}\int_0^{\infty}\frac{dz}{z^{3/2}}\left\{\cos\left[xz-\frac{\pi}{4}-\frac{z^3}{v+4}\right]-\cos\left[xz-\frac{\pi}{4}\right]\right\}. \tag{E2}$$

In the integral Eq. (7.24), we perform the following change of variables:

$$\rho_1=\frac{z}{2}\left(1+\sqrt{\frac{v+4}{v}}\right),\qquad \rho_2=\frac{z}{2}\left(\sqrt{\frac{v+4}{v}}-1\right), \tag{E3}$$

after which it acquires the form

$$P_1^-(x)=\frac{3(2^{13/6})}{\pi^{3/2}}\int_0^{\infty}\frac{dv}{(v+4)^{1/2}}\int_0^{\infty}\frac{dz}{z^{3/2}}\left\{\cos\left[xz+\frac{\pi}{4}+\frac{z^3}{v}\right]-\cos\left[xz+\frac{\pi}{4}\right]\right\}. \tag{E4}$$

It is convenient to present $\int_0^{\infty}dv$ in Eq. (E4) as the following difference of integrals:

$$P_1^-(x)=\frac{3(2^{13/6})}{\pi^{3/2}}\int_0^{\infty}\frac{dz}{z^{3/2}}\left(-\int_{-4}^{0}\frac{dv}{\sqrt{v+4}}+\int_{-4}^{\infty}\frac{dv}{\sqrt{v+4}}\right)\times\left(\cos\left[xz+\frac{\pi}{4}+\frac{z^3}{v}\right]-\cos\left[xz+\frac{\pi}{4}\right]\right). \tag{E5}$$

We now observe that the the second term cancels *identically* the function $P_+$. Then we readily arrive to Eq. (7.25).

## APPENDIX F: ASYMPTOTICS OF THE DENSITY OF STATES

The idea of derivation of Eq. (8.9) from Eq. (8.10) is that the major contribution to the integral Eq. (8.10) comes from the domain $|\rho_2-\rho_1|\ll\rho_1,\rho_2$, i.e., from the domain where $\rho_1$ and $\rho_2$ are close to each other. To make use of this simplification, we rewrite the argument of the cosine in Eq. (8.10) as

$$\frac{(\rho_1+\rho_2)^3}{4}+\frac{\pi}{4}-\frac{2^{7/3}\omega}{\omega_h}(\rho_1+\rho_2)-\frac{(\rho_1+\rho_2)(\rho_2-\rho_1)^2}{4}, \tag{F1}$$

where we had introduced $\omega_h=\omega_0(h/h_0)^{2/3}$. It is seen from Eq. (F1) that the typical value of $(\rho_2+\rho_1)$ is $(\omega/\omega_h)^{1/2}\gg 1$, while the typical value of $(\rho_2-\rho_1)$ is $(\rho_2+\rho_1)^{-1/2}\sim(\omega/\omega_h)^{-1/4}$, i.e., the relevant difference $\rho_2-\rho_1$ is small indeed. This allows us to extend the integration over $\rho_2-\rho_1$ from zero to infinity and perform the integral. This yields

$$\left\langle\frac{\delta\nu(\omega)}{\nu_0}\right\rangle=-\frac{(\nu_0 V)^3\omega\omega_h^{1/2}}{\pi^{1/2}E_F^{3/2}}\int_0^\infty\frac{d\rho}{\rho^3}\left\langle\cos\left[\frac{\rho^3}{4}-2^{7/3}\rho\frac{\omega}{\omega_h}\right]\right\rangle. \tag{F2}$$

The argument of the cosine in Eq. (F2) has a sharp minimum at $\rho=\rho_0=(2^{13/6}/3^{1/2})\sqrt{\omega/\omega_h}$, which allows us to perform the integration over $\rho$ by introducing $\delta\rho=\rho-\rho_0$ and extending the integration over $\delta\rho$ from minus to plus infinity. This yields the following asymptote of $\delta\nu(\omega)$:

$$\left\langle\frac{\delta\nu(\omega)}{\nu_0}\right\rangle=-\frac{1}{64(2^{7/12})\sqrt{\pi}}\frac{(\nu_0 V)^3\omega_h^{9/4}}{E_F^{3/2}\omega^{3/4}}\left\langle\sin\left[\frac{32\sqrt{2}}{3\sqrt{3}}\left(\frac{\omega}{\omega_h}\right)^{3/2}+\frac{\pi}{4}\right]\right\rangle_{h(x,y)}, \tag{F3}$$

in which the random magnetic field enters through $\omega_h$. The argument of the sine contains the term $\propto\omega_h^{-3/2}$, which can be presented as $sh_0/h$, where the constant $s$ is equal to $16(2\omega/3\omega_0)^{3/2}$. The factor in front of the sine contains $\omega_h^{9/4}\propto h^{3/2}$. Then, the Gaussian averaging over $h$ can be carried out analytically using the fact that $s\gg 1$. This yields

$$\left\langle h^{3/2}\sin\left[\frac{sh_0}{h}+\frac{\pi}{4}\right]\right\rangle_{h(x,y)}=\frac{h_0^{3/2}s^{1/2}}{\sqrt{6}}\sin\left(\frac{3^{3/2}s^{2/3}}{2^{5/3}}\right)\exp\left\{-\frac{3s^{2/3}}{2^{5/3}}\right\}. \tag{F4}$$

Combining Eqs. (F4) and (F3), one reproduces Eq. (8.9) of the main text.


[1] B. L. Altshuler and A. G. Aronov, Solid State Commun. **30**, 115 (1979).
[2] B. L. Altshuler, A. G. Aronov, and P. A. Lee, Phys. Rev. Lett. **44**, 1288 (1980).
[3] A. M. Rudin, I. L. Aleiner, and L. I. Glazman, Phys. Rev. B **55**, 9322 (1997).
[4] E. G. Mishchenko and A. V. Andreev, Phys. Rev. B **65**, 235310 (2002).
[5] B. L. Altshuler and L. B. Ioffe, Phys. Rev. Lett. **69**, 2979 (1992).
[6] D. V. Khveshchenko and S. V. Meshkov, Phys. Rev. B **47**, 12051 (1993).
[7] M. U. Ubbens and P. A. Lee, Phys. Rev. B **49**, 13049 (1994).
[8] J. K. Jain, Phys. Rev. Lett. **63**, 199 (1989); **40**, 8079 (1989); **41**, 7653 (1990).
[9] B. I. Halperin, P. A. Lee, and N. Read, Phys. Rev. B **47**, 7312 (1993).
[10] A. K. Geim, S. V. Dubonos, and A. V. Khaetskii, JETP Lett. **51**, 121 (1990).
[11] S. J. Bending, K. von Klitzing, and K. Ploog, Phys. Rev. Lett. **65**, 1060 (1990).
[12] A. K. Geim, S. J. Bending, and I. V. Grigorieva, Phys. Rev. Lett. **69**, 2252 (1992).
[13] A. K. Geim, S. J. Bending, I. V. Grigorieva, and M. G. Blamire, Phys. Rev. B **49**, 5749 (1994).
[14] A. Smith, R. Taboryski, L. T. Hansen, C. B. Sørensen, Per Hedegård, and P. E. Lindelof, Phys. Rev. B **50**, 14726 (1994).
[15] F. B. Mancoff, R. M. Clarke, C. M. Marcus, S. C. Zhang, K. Campman, and A. C. Gossard, Phys. Rev. B **51**, 13269 (1995).
[16] G. M. Gusev, U. Gennser, X. Kleber, D. K. Maude, J. C. Portal, D. I. Lubyshev, P. Basmaji, M. de P. A. Silva, J. C. Rossi, and Y. V. Nastaushev, Phys. Rev. B **53**, 13641 (1996).
[17] A. A. Bykov, G. M. Gusev, J. R. Leite, A. K. Bakarov, N. T. Moshegov, M. Cassé, D. K. Maude, and J. C. Portal, Phys. Rev. B **61**, 5505 (2000).
[18] A. W. Rushforth, B. L. Gallagher, P. C. Main, A. C. Neumann, M. Henini, C. H. Marrows, and B. J. Hickey, Phys. Rev. B **70**, 193313 (2004).
[19] A. G. Aronov, A. D. Mirlin, and P. Wölfle, Phys. Rev. B **49**, 16609 (1994).
[20] D. K. K. Lee and J. T. Chalker, Phys. Rev. Lett. **72**, 1510 (1994).
[21] D. K. K. Lee, J. T. Chalker, and D. Y. K. Ko, Phys. Rev. B **50**, 5272 (1994).
[22] D. B. Chklovskii and P. A. Lee, Phys. Rev. B **48**, 18060 (1993).
[23] D. B. Chklovskii, Phys. Rev. B **51**, 9895 (1995).
[24] V. I. Fal'ko, Phys. Rev. B **50**, 17406 (1994).
[25] D. V. Khveshchenko, Phys. Rev. Lett. **77**, 1817 (1996).
[26] A. D. Mirlin, D. G. Polyakov, and P. Wölfle, Phys. Rev. Lett. **80**, 2429 (1998).
[27] A. D. Mirlin, J. Wilke, F. Evers, D. G. Polyakov, and P. Wölfle, Phys. Rev. Lett. **83**, 2801 (1999).
[28] A. D. Mirlin, D. G. Polyakov, F. Evers, and P. Wölfle, Phys. Rev. Lett. **87**, 126805 (2001).
[29] A. V. Izyumov and B. D. Simons, J. Phys. A **32**, 5563 (1999).
[30] A. Shelankov, Phys. Rev. B **62**, 3196 (2000).
[31] H. Mathur and H. U. Baranger, Phys. Rev. B **64**, 235325 (2001).
[32] K. B. Efetov and V. R. Kogan, Phys. Rev. B **70**, 195326 (2004).
[33] B. L. Altshuler, A. G. Aronov, and D. E. Khmelnitsky, J. Phys. C **15**, 7367 (1982).
[34] A. G. Aronov and P. Wölfle, Phys. Rev. B **50**, 16574 (1994).
[35] A. G. Aronov and P. Wölfle, Phys. Rev. Lett. **72**, 2239 (1994).
[36] A. V. Chubukov, D. L. Maslov, S. Gangadharaiah, and L. I. Glazman, Phys. Rev. B **71**, 205112 (2005).
[37] J. Friedel, Nuovo Cimento, Suppl. **7**, 287 (1958).
[38] P. G. de Gennes, J. Phys. Radium **23**, 630 (1962).
[39] P. F. de Chatel, J. Magn. Magn. Mater. **23**, 28 (1981).
[40] A. Y. Zyuzin and B. Z. Spivak, JETP Lett. **43**, 234 (1986).
[41] L. N. Bulaevskii and S. V. Panyukov, JETP Lett. **43**, 240 (1986).
[42] A. Jagannathan, E. Abrahams, and M. J. Stephen, Phys. Rev. B

**37**, 436 (1988).
[43] I. V. Lerner, Phys. Rev. B **48**, 9462 (1993).
[44] J. A. Sobota, D. Tanaskovic, V. Dobrosavljevic, Phys. Rev. B **76**, 245106 (2007).
[45] Y. Hasegawa and Ph. Avouris, Phys. Rev. Lett. **71**, 1071 (1993).
[46] M. Ono, Y. Nishigata, T. Nishio, T. Eguchi, and Y. Hasegawa, Phys. Rev. Lett. **96**, 016801 (2006).
[47] Y. Hasegawa, M. Ono, Y. Nishigata, T. Nishio, and T. Eguchi, J. Phys.: Conf. Ser. **61**, 399 (2007).
[48] M. F. Crommie, C. P. Lutz, and D. M. Eigler, Nature (London) **363**, 524 (1993).
[49] A. Yazdani, B. A. Jones, C. P. Lutz, M. F. Crommie, and D. M. Eigler, Science **275**, 1767 (1997).
[50] M. C. M. M. van der Wielen, A. J. A. van Roij, and H. van Kempen, Phys. Rev. Lett. **76**, 1075 (1996).
[51] Ph. Hofmann, B. G. Briner, M. Doering, H.-P. Rust, E. W. Plummer, and A. M. Bradshaw, Phys. Rev. Lett. **79**, 265 (1997).
[52] J. E. Hoffman, K. McElroy, D.-H. Lee, K. M. Lang, H. Eisaki, S. Uchida, and J. C. Davis, Science **297**, 1148 (2002).
[53] P. T. Sprunger, L. Petersen, E. W. Plummer, E. Lægsgaard, and F. Besenbacher, Science **275**, 1764 (1997).
[54] Q.-H. Wang and D.-H. Lee, Phys. Rev. B **67**, 020511(R) (2003).
[55] G. F. Giuliani and G. E. Simion, Solid State Commun. **127**, 789 (2003).
[56] J. Fransson and A. V. Balatsky, Phys. Rev. B **75**, 195337 (2007).
[57] A. M. Tsvelik, Phys. Rev. B **77**, 073402 (2008).
[58] T. A. Sedrakyan, E. G. Mishchenko, and M. E. Raikh, Phys. Rev. Lett. **99**, 036401 (2007).
[59] F. Stern, Phys. Rev. Lett. **18**, 546 (1967).
[60] A. V. Chubukov and D. L. Maslov, Phys. Rev. B **68**, 155113 (2003).
[61] A. V. Chubukov and D. L. Maslov, Phys. Rev. B **69**, 121102(R) (2004).
[62] L. P. Gor'kov, Sov. Phys. JETP **9**, 1364 (1959).
[63] I. L. Aleiner and L. I. Glazman, Phys. Rev. B **52**, 11296 (1995).
[64] T. A. Sedrakyan, E. G. Mishchenko, and M. E. Raikh, Phys. Rev. Lett. **99**, 206405 (2007).
[65] A. V. Chubukov, D. L. Maslov, S. Gangadharaiah, and L. I. Glazman, Phys. Rev. Lett. **95**, 026402 (2005).
[66] S. Gangadharaiah, D. L. Maslov, A. V. Chubukov, and L. I. Glazman, Phys. Rev. Lett. **94**, 156407 (2005).
[67] R. L. Willett, K. W. West, and L. N. Pfeiffer, Phys. Rev. Lett. **75**, 2988 (1995).
[68] R. R. Du, H. L. Stormer, D. C. Tsui, L. N. Pfeiffer, and K. W. West, Solid State Commun. **90**, 71 (1994); Phys. Rev. Lett. **70**, 2944 (1993).
[69] D. R. Leadley, M. van der Burgt, R. J. Nicholas, C. T. Foxon, and J. J. Harris, Phys. Rev. Lett. **72**, 1906 (1994); Phys. Rev. B **53**, 2057 (1996).
[70] P. T. Coleridge, Z. W. Wasilewski, P. Zawadzki, A. S. Sachrajda, and H. A. Carmona, Phys. Rev. B **52**, R11603 (1995).
[71] L. P. Rokhinson and V. J. Goldman, Phys. Rev. B **56**, R1672 (1997).
[72] Song He, P. M. Platzman, and B. I. Halperin, Phys. Rev. Lett. **71**, 777 (1993).
[73] A. V. Shytov, L. S. Levitov, and B. I. Halperin, Phys. Rev. Lett. **80**, 141 (1998).
[74] L. S. Levitov, A. V. Shytov, and B. I. Halperin, Phys. Rev. B **64**, 075322 (2001).
[75] M. Grayson, D. C. Tsui, L. N. Pfeiffer, K. W. West, and A. M. Chang, Phys. Rev. Lett. **80**, 1062 (1998).
[76] A. M. Chang, M. K. Wu, C. C. Chi, L. N. Pfeiffer, and K. W. West, Phys. Rev. Lett. **86**, 143 (2001).
[77] J. A. Hertz, Phys. Rev. B **14**, 1165 (1976).
[78] A. J. Millis, Phys. Rev. B **48**, 7183 (1993).
[79] D. Belitz and T. R. Kirkpatrick, Phys. Rev. Lett. **89**, 247202 (2002).
[80] A. V. Chubukov, C. Pépin, and J. Rech, Phys. Rev. Lett. **92**, 147003 (2004).
[81] J. Rech, C. Pépin, and A. V. Chubukov, Phys. Rev. B **74**, 195126 (2006).
[82] H. v. Löhneysen, A. Rosch, M. Vojta, and P. Wölfle, Rev. Mod. Phys. **79**, 1015 (2007).
[83] I. Paul, C. Pépin, B. N. Narozhny, and D. L. Maslov, Phys. Rev. Lett. **95**, 017206 (2005).
[84] I. Paul, arXiv:0709.1140 (unpublished).
[85] By making this assumption we, disregard the fact that the change of *orientation* of local magnetization, $\mathbf{S}(\mathbf{r})$, *without change of the magnitude* also leads to the curving of electron trajectories; see Y. Aharonov and A. Stern, Phys. Rev. Lett. **69**, 3593 (1992).
[86] O. Vallée and M. Soares, *Airy Functions and Applications to Physics* (World Scientific, Hackensack, NJ, 2004).